A CASE STUDY

on the use of VLF, Magnetics and airborne TEM

For Gold and VMS Exploration in Northern Canada

May 2018

Stephen L. Masson P. Geo. M.Sc.
Copper Reef Mining Corporation
12 Mitchell Rd.
Flin Flon, MB

R.W. Groom , PhD
Petros Eikon Incorporated
Orangeville, ON

Richard Masson
Copper Reef Mining Corporation
12 Mitchell Rd.
Flin Flon, MB

Summary

This study contains the analyses of ground magnetic and VLF data in combination with airborne time domain electromagnetic and magnetic data. In particular, the survey was for the purpose of identifying and predicting the extension of a stress zone known to contain gold deposits. The utilizes 3D modeling of VLF, magnetics and airborne TEM data to quantify the geophysical targets. EMIGMA software was utilized and in particular the implementation of the LN approximator as well as a relatively new plate modeling algorithm. Additionally, 3D magnetic modeling is also utilized to understand the local structures. This, magnetic inversion allows joint inversion of ground and airborne data and utilizes a Trust Region optimization algorithm.

In the process of studying the data for the original intentions of the survey, an airborne TEM anomaly was identified, resolved and modeled and determined to be a likely VMS structure.

Introduction

During the days of October 5, 2017 to February 28, 2018 M'Ore Exploration Services refurbished and extended the metric grid by line cutting and chaining covering the Alberts Lake Gold Shear Zone. J.D Sigfrid and Associates Ltd. completed a Very Low Frequency Electromagnetic (VLF-EM) and ground magnetic survey in the Alberts Lake area. Both the VLF and magnetometer field readings were taken at 12.5 m station intervals along east-west section lines spaced 25 m apart. The claims are shown in Figure 1.

The VLF-EM coverage consisted of 12.95 line-kilometers of in-phase and quadrature component data measured using GEM systems GSM-19 units tuned to transmitters based in Seattle, Wa. (NLK: 24.8 kHZ) and Cutler, MA. (NSS: 24.0 kHz). The entire grid was surveyed with both transmitters in order to utilize both source polarizations to interpret structures. As the source polarizations are almost orthogonal, no geological structure will be decoupled from both sources.

The magnetometer coverage consisted of 12.95 line-kilometers of total field intensity data collected with GEM systems GSM-19 overhauser (memory) field magnetometer as a rover with a GSM-19T proton precession magnetometer utilized for the basestation data at two stations. The rover data was partially corrected for variation and noise by automatic procedures in the GSM-19. The two sets of basestation data for each day were merged. High frequency variations and outliers were removed and the results averaged for the two stations to produce the final base station data for correction of the rover data. The magnetic data was analyzed and interpreted by Petros Eikon Incorporated as was the VLF data. Airborne VTEM data for both EM and magnetic data was analyzed and interpreted within the region of the grid.

Magnetic Data Quality and Processing

Data were collected on 3 days, January 9, 10 and 17 with a GEM Overhauser magnetometer not equipped with internal GPS on lines roughly orientated 36 degrees west of north. Station spacing was nominally 12.5m and line spacing 25m. 1073 unique stations were collected within the grid.

The UTM locations of the stations was generated by taking the GPS measurement at the ends of the lines and the UTM positions of the intermediate stations determined by interpolating assuming a uniform 12.5m spacing between each stations (Figure 3). UTM projections are NAD83, zone 14N.

Some repeat measurements were taken at a small number of stations. However, all repeats indicated that the measurements were repeatable in a resolution suitable for such a survey.
Dual basestations just outside the grid were used to correct variations. Small changes in basestation data attributed to spherics were removed via filtering. The data from the 2 base stations was average to produce the data to correct the rover data for the diurnal and long wavelength external signal. Spatial IGRF corrections were made for each day. All data were examined individually to find repeats. Outliers were removed and then repeats stacked to produce the reduced total magnetic intensity (TMI).

Figure 3 displays the location of all the stations with a satellite map underlain. The only significant surficial feature is a small lake in the NE section of the grid. The reader will note that not all lines are parallel. While this does alter the spatial sampling of the magnetic response, this issue poses no problems for interpretation. The average IGRF for the 3 days is approximately 58,000nT which is very close to the mean response in the pink colors which dominate the map. Particularly in the NW of the grid, there are obviously stations of high response due to surficial rocks but the main response in the NW is significant at about 1,000nT. The minimum data is 57,205nT while the maximum is 69,450nT.

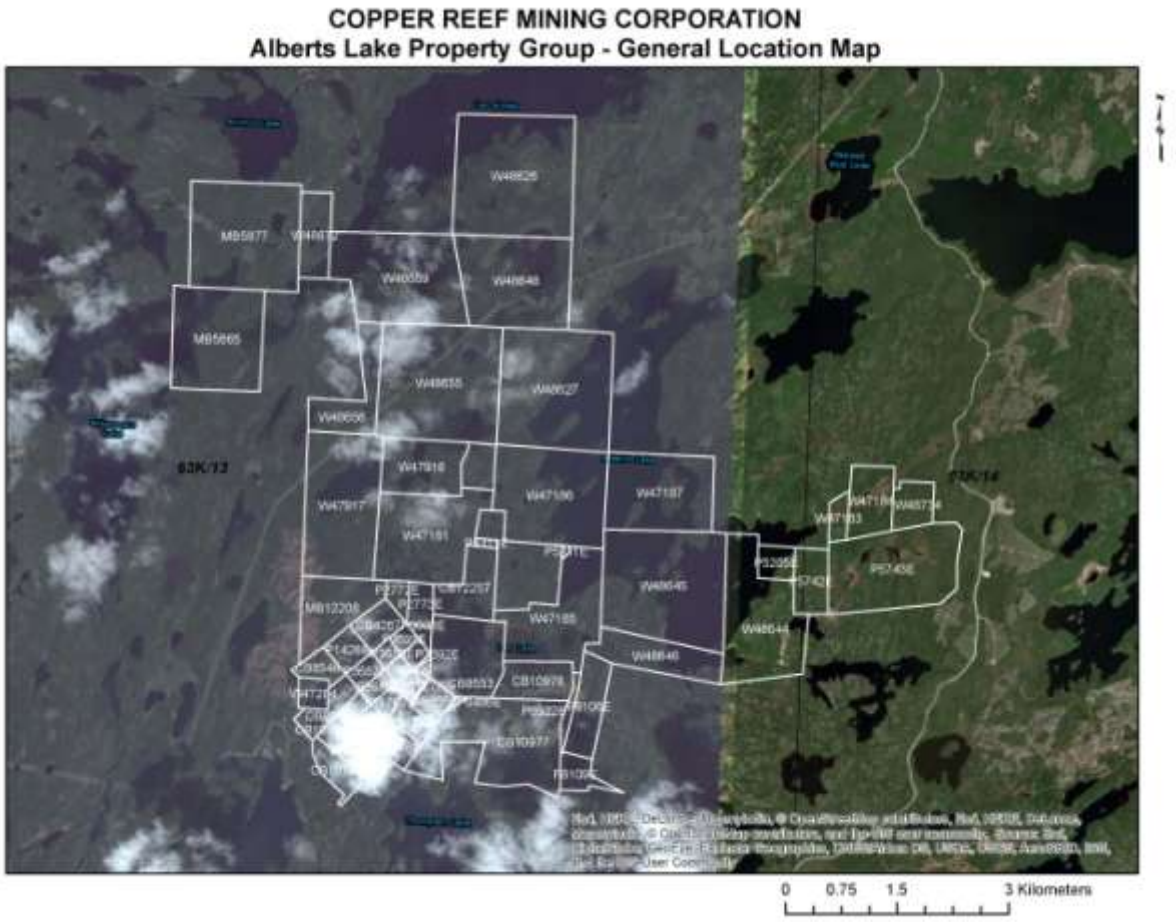

Figure 1: Claim Location Map

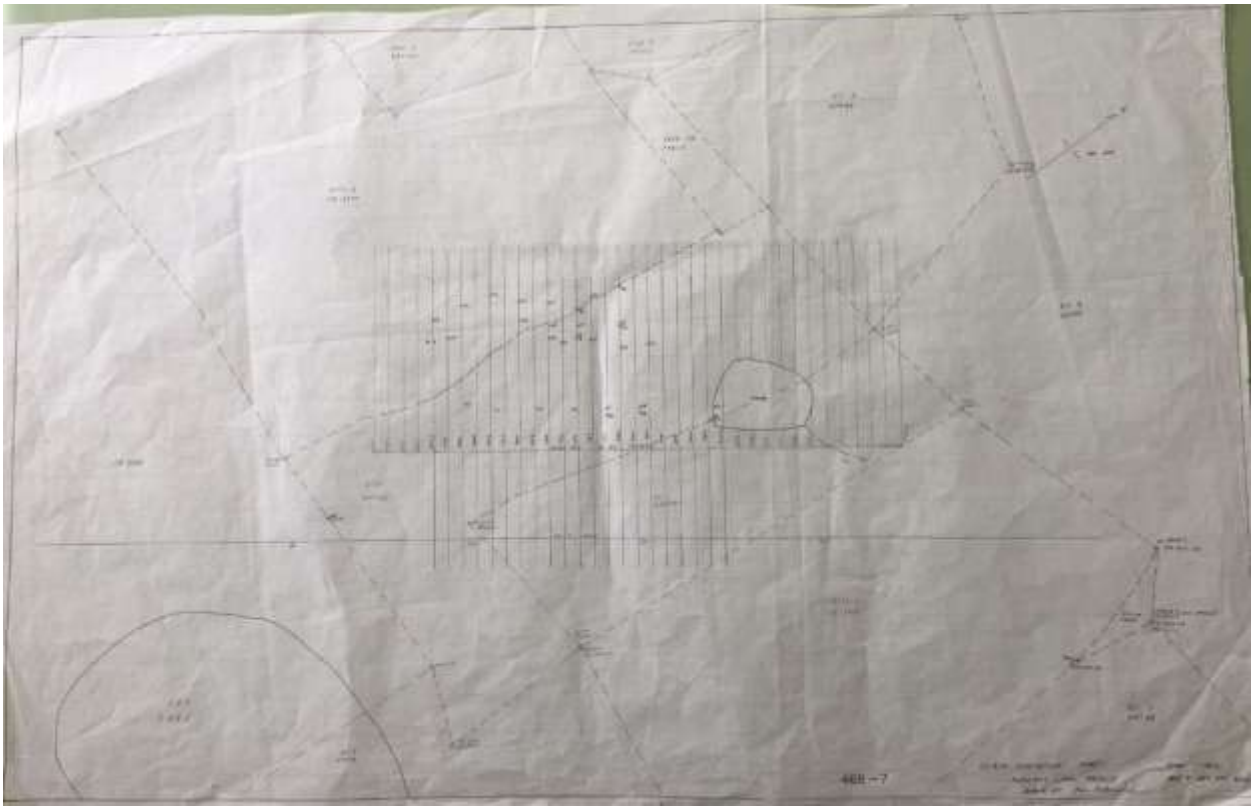

Figure 2: Claim Area of Mag/VLF geophysical survey over cut metric grid

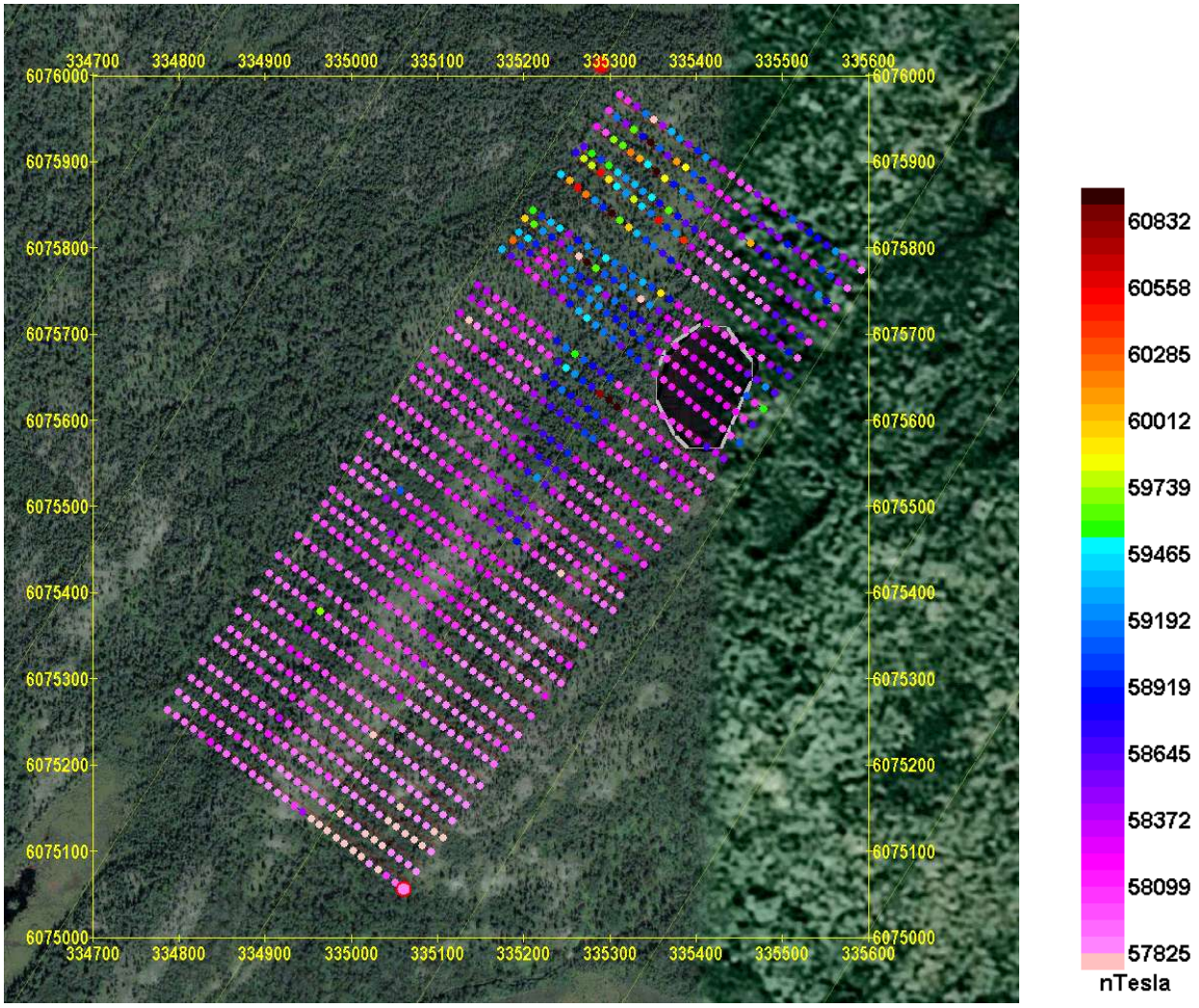

Figure 3: Magnetic and VLF data stations. NAD83 datum

Data Quality: From the small number of repeats, we would conclude the data is good and there is very little noise present. However, there appears to be a great many small features that are too small to carry across profiles indicating shallow occurrences. Below, we plot (Figure 4) two neighbouring profiles. The top figure is 2 lines in the north (L225, L225) and below 3 lines in the south (L-25, L-50 and L-75).

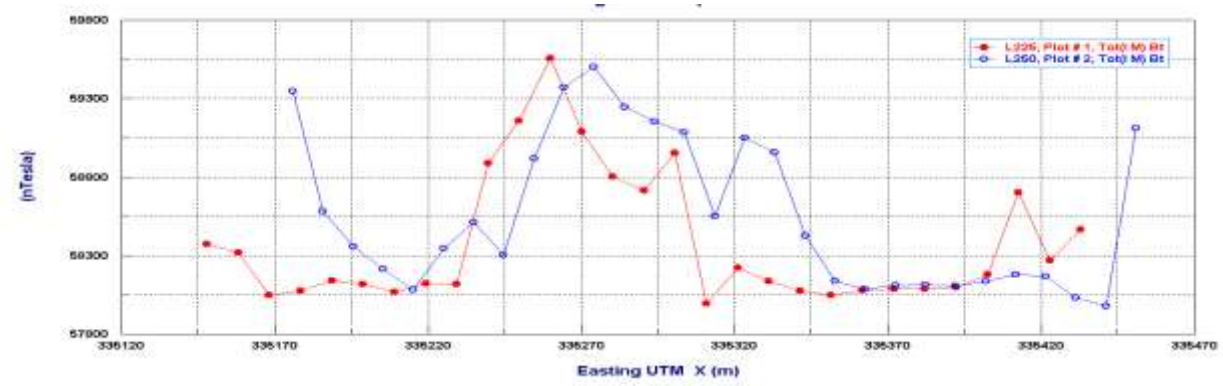

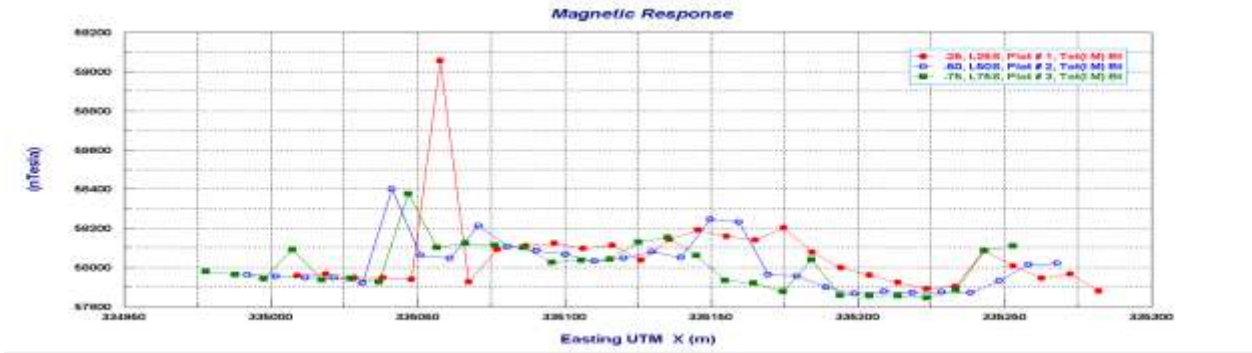

Figure 4: Data examples for 5 lines. Top figure: 2 consecutive lines in the north. Bottom figure: 3 consecutive lines in the south.

For all data grids, cells of 6m along profile and 12.5m across profiles are used to maintain the resolution along the profiles. In Figure 5, we present the data gridded and then contoured. The distribution of data with amplitude is shown to the right of the legend.

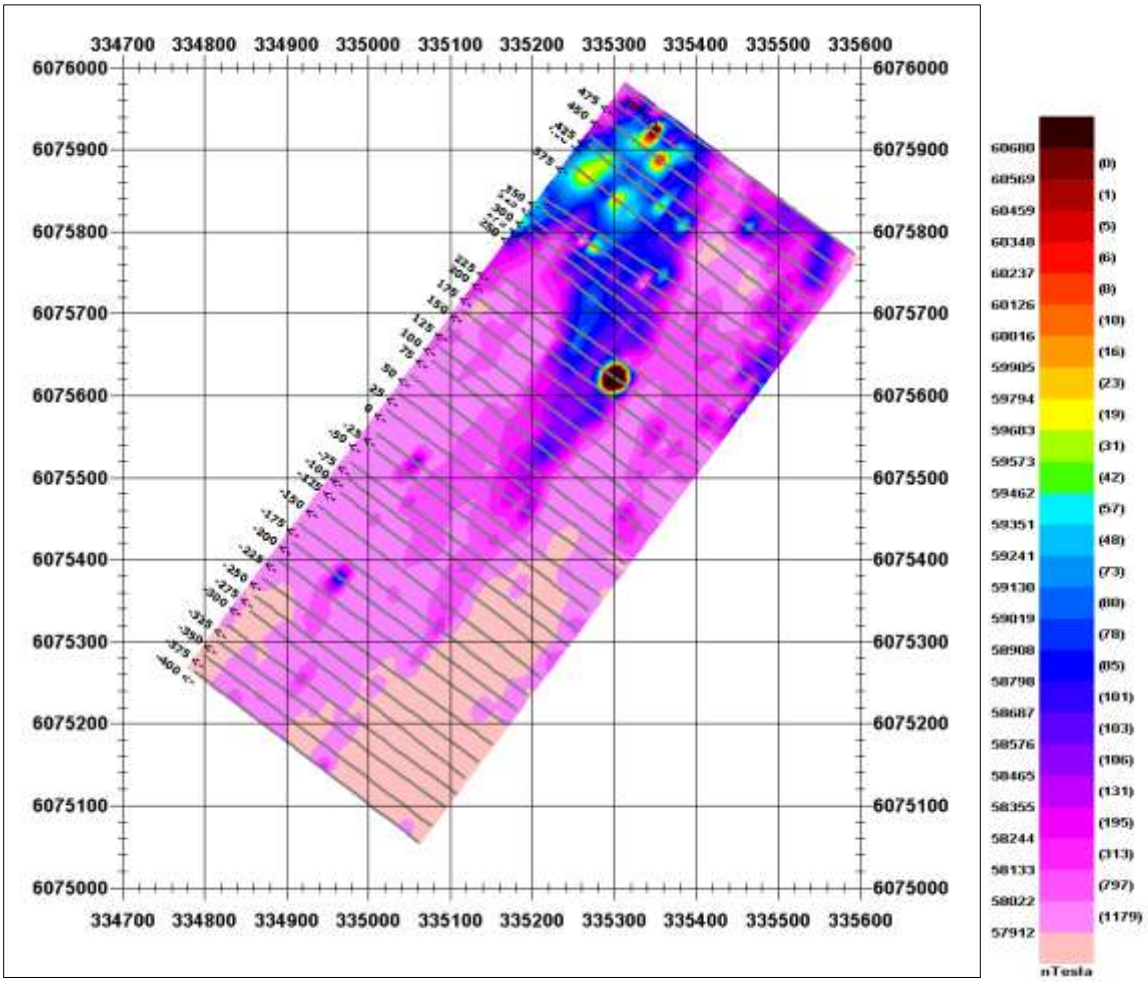

Figure 5: Contoured ground magnetic data

Primary Features of the Magnetic Data:

The data has an exceptionally large variation of more than 10,000 nT. However, the majority of the data falls into two ranges. The majority of the data is near the IGRF which means little local magnetization between 57,200 nT and 58,200 nT. The most prominent anomalous feature is the data in the range of 58,400nT and 59,200nT. The latter is a high to the NW while there is a Low to the SE but this is a very minimal low. There is an apparent boundary running perpendicular to the grid lines. There are some small areas of very high response and in particular a very high response on Line 200N. Surface sampling at the locations could prove useful.

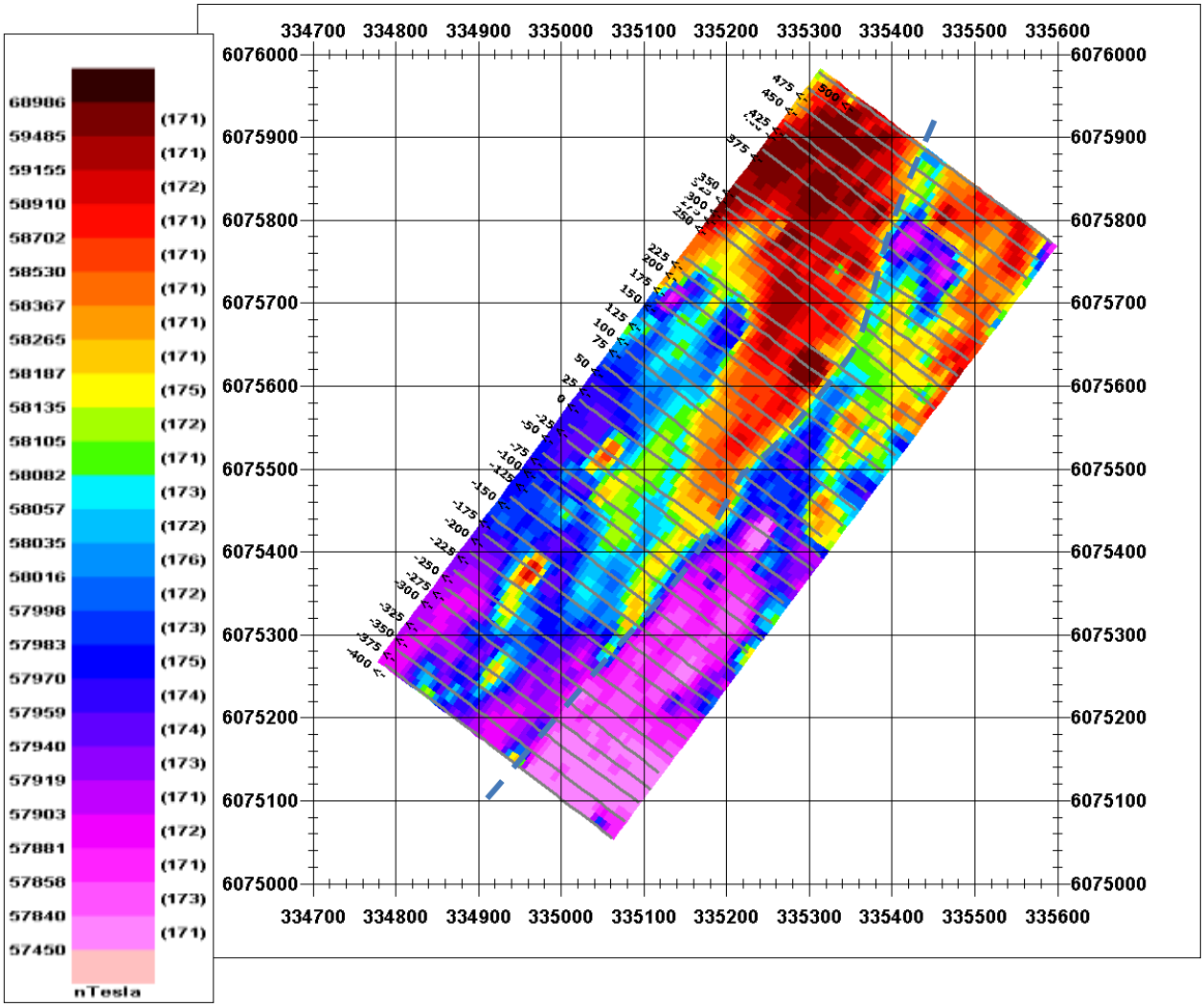

Figure 6: Equal weight magnetic data with structural boundary

In Figure 6, we have displayed the magnetic data by equal weight. In this image, the boundaries are most obvious. We have outlined a boundary by a broken black line to represent a boundary that we feel is structurally important. In Figure 7, the horizontal derivative along the profile is

displayed. This display shows more clearly the magnetic structures and boundaries. Our interpretation of the major fracture is now shown in yellow.

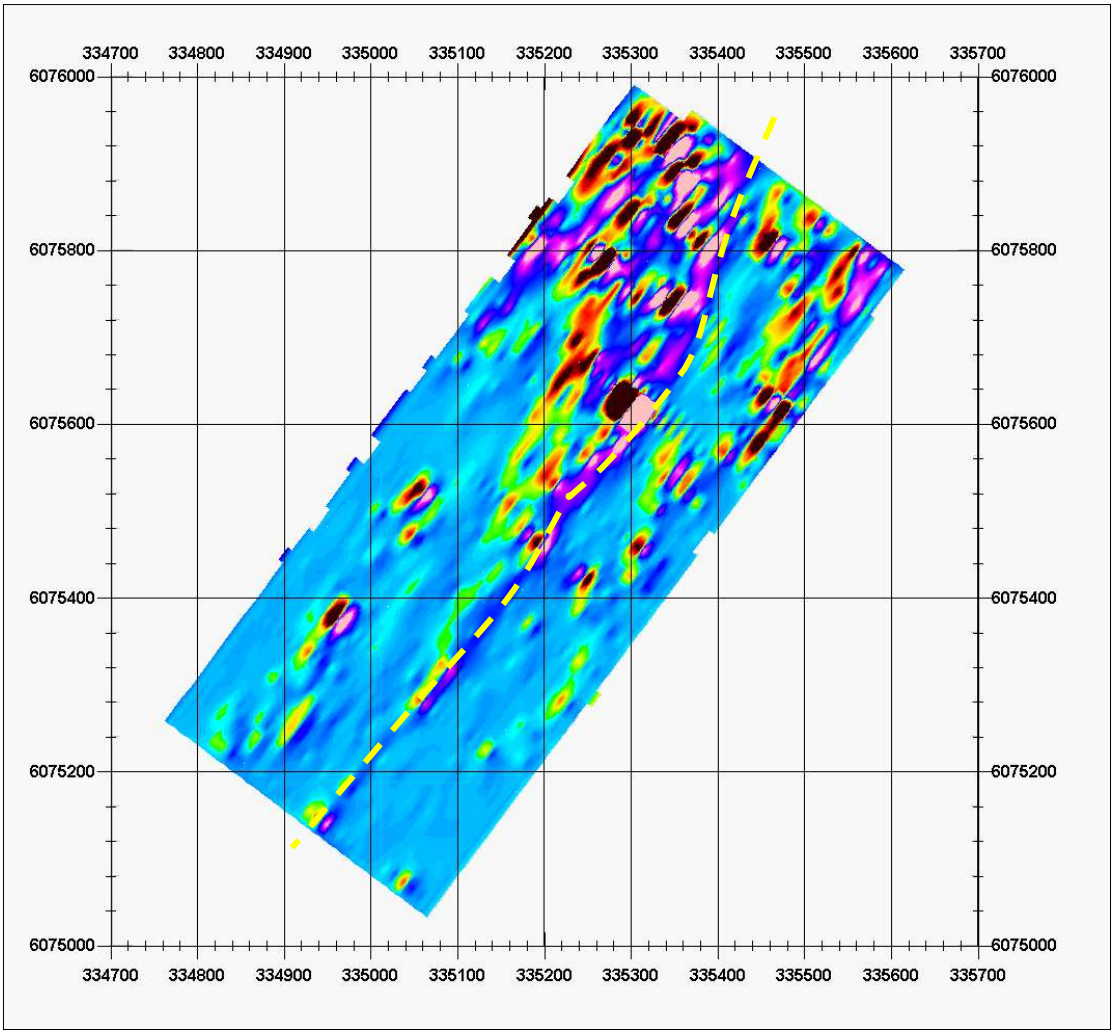

Figure 7: In line horizontal derivative of the ground magnetic data.

Magnetic Data Analyses

In Figure 8, we contour the magnetic data reducing the range to highlight the variations. The local geology and presented by Manitoba government geologists is underlain. The hypothesized structural boundary running down the middle of the grid is outline in a broken pink line. This boundary is displaced from the government mapped Albert's Lake fault by approximately 90m to the NW (Fig 8).

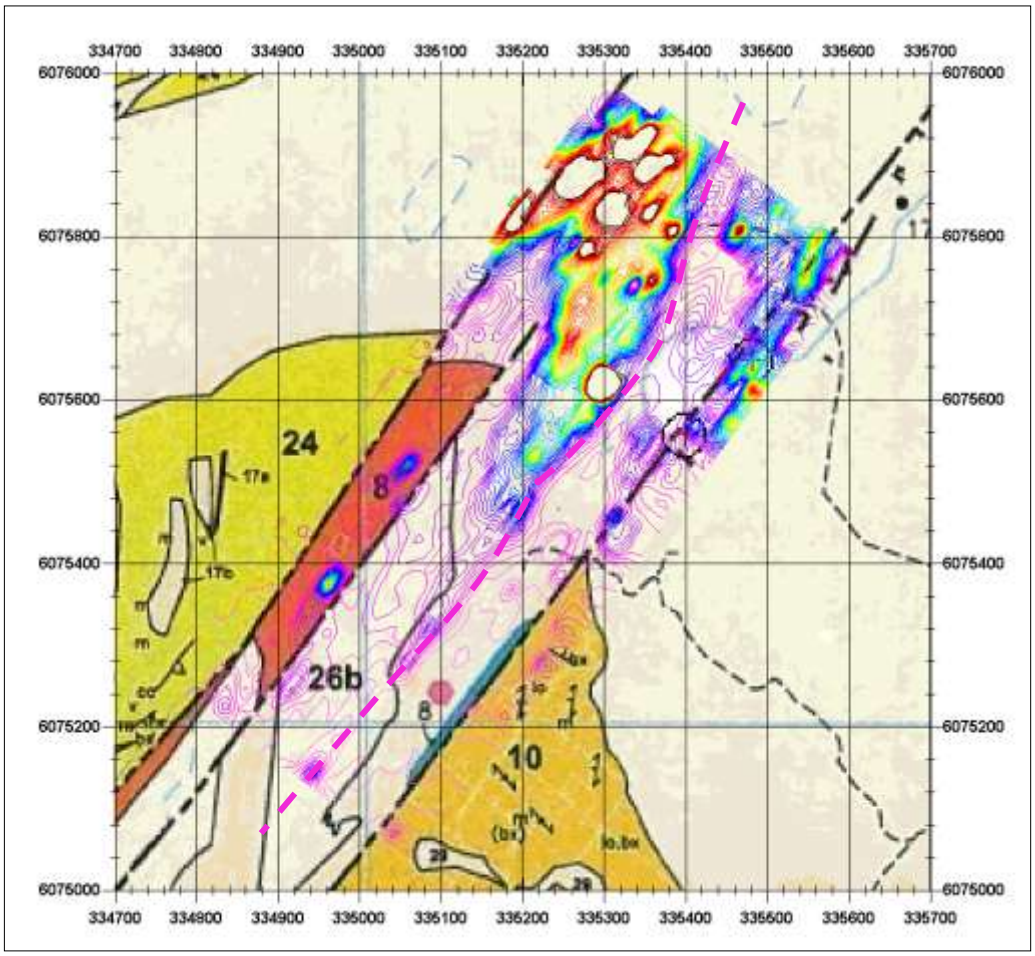

Figure 8: Magnetic data with geology underlain

3D Magnetic Inversion of the Ground Magnetic Data

3D Inversion: For the 3D magnetic inversion, we have determined via trials that the survey "sees" no deeper" than 250m. Thus, we have performed inversions without constraint to this depth. In the figures below (Figures 9a-9c), we view the inversion cut along lines perpendicular to the profile directions.

Here, we view the susceptibility as logarithmic as it better visually outlines the structures. The display is such that horizontal and vertical scaling are identical.

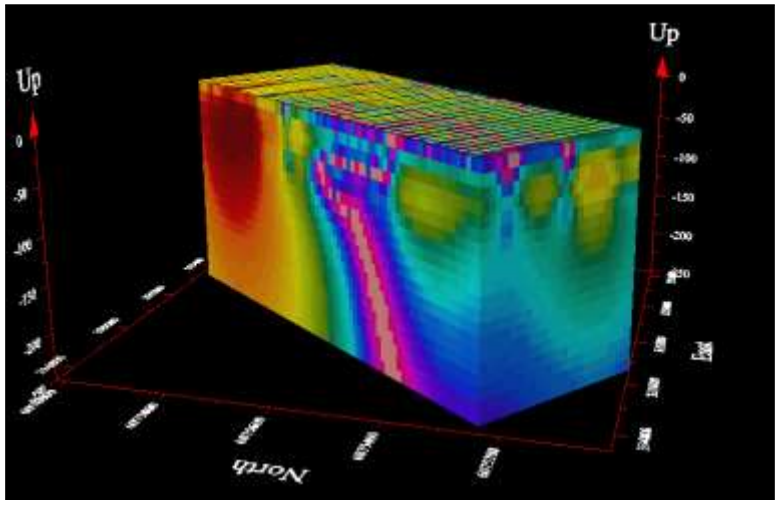

Figure 9a: 3D inversion on western edge viewed from the SW.

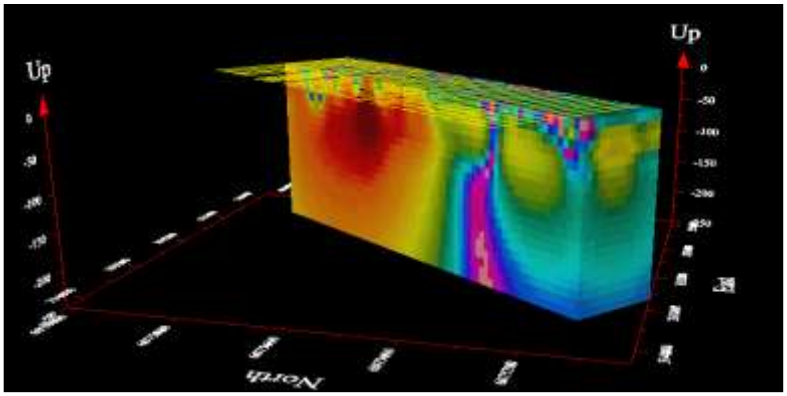

Figure 9b: 3D inversion down center viewed from the SW

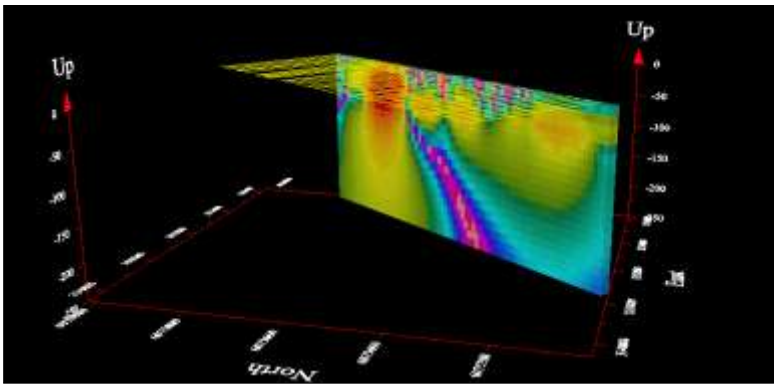

Figure 9c: 3D inversion on eastern edge viewed from the SW

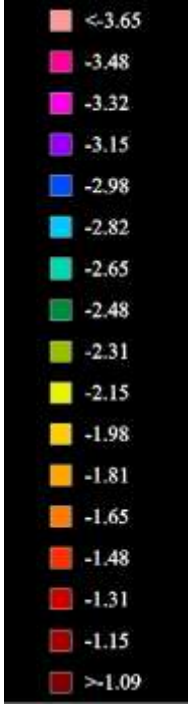

3D Inversions of ground magnetics: 2D Cross Section slices parallel to strike

The inversion volume is 950m long by 400m wide using 12.5m cells and has a depth of 250m also using a cell thickness of 12.5m. The angle of the grid is 37 degrees east of north and the following slices are therefore at this angle along the entire grid down to 250m depth.

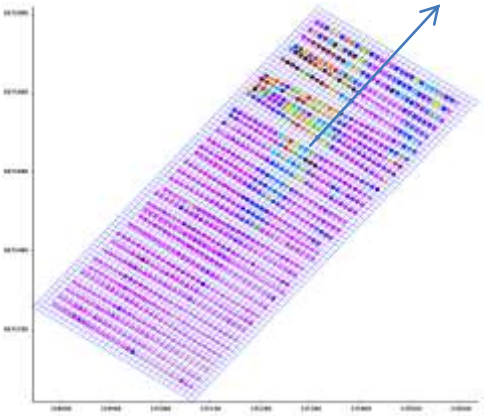

Figure 10: Magnetic survey showing strike of 3D inversion grid and angle of sections

To explain the inversion sections, we use the example below (Fig11). As this is a section parallel to the long axis of the inversion grid (strike), the coordinates at the top of the plot are the northing. To understand where this section is taken, the easting for the south end is shown on the left and the easting for the northing end on the south. Thus, this section is taken from the eastern edge of the inversion model.

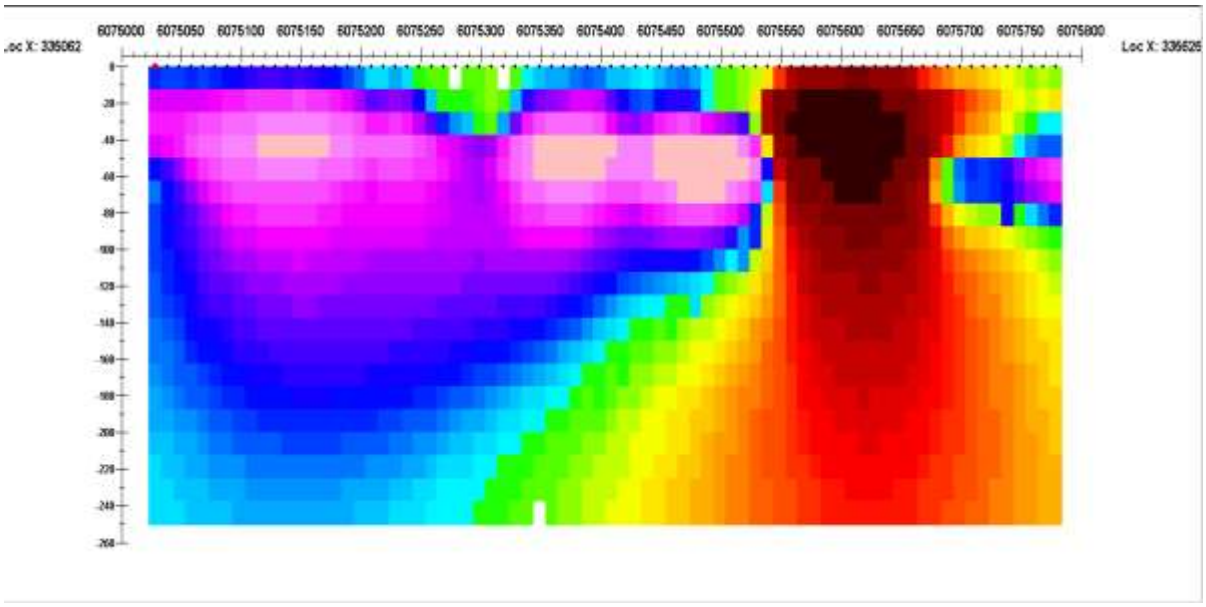

Figure 11: Inversion selection parallel to strike (37 degrees east of north)

We will now present 8 longitudinal slices of the inversion model, starting from the western face of the grid and proceeding through the grid to the eastern edge. These slices are not at regular intervals but rather when there occurs a significant change in the structure occurs.

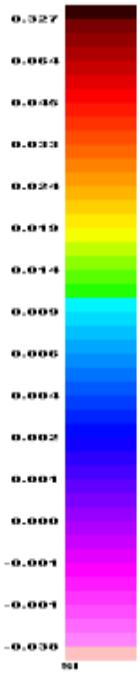

What is observed (Fig 12) is that the magnetic anomaly shown in the surface data is due to a relatively strong magnetic structure which is dipping to the south and to the east?

Figure 12: Inversion sections parallel to strike western portion of magnetic survey

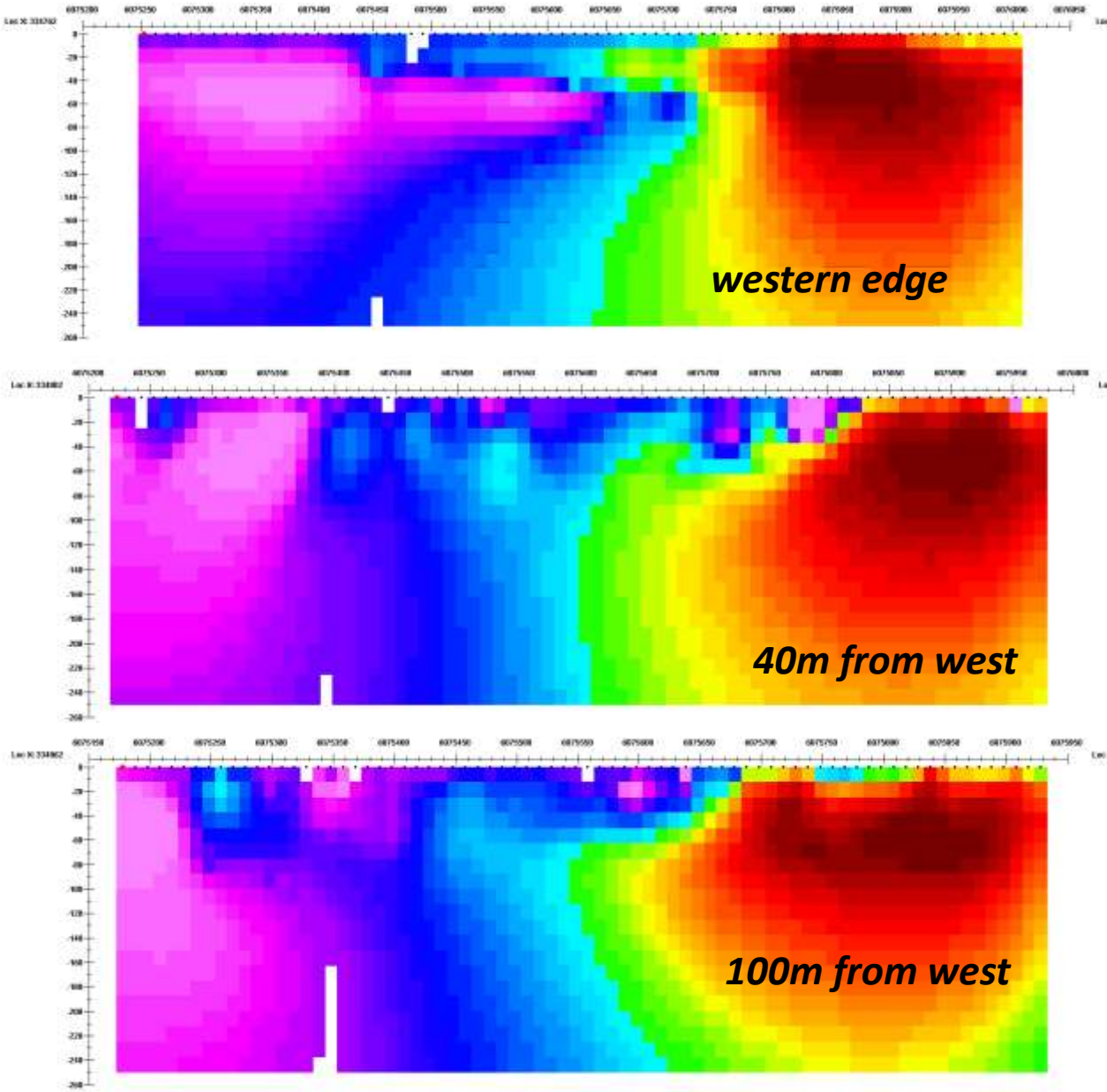

Figure 13: Inversion sections parallel to strike eastern portion of magnetic survey

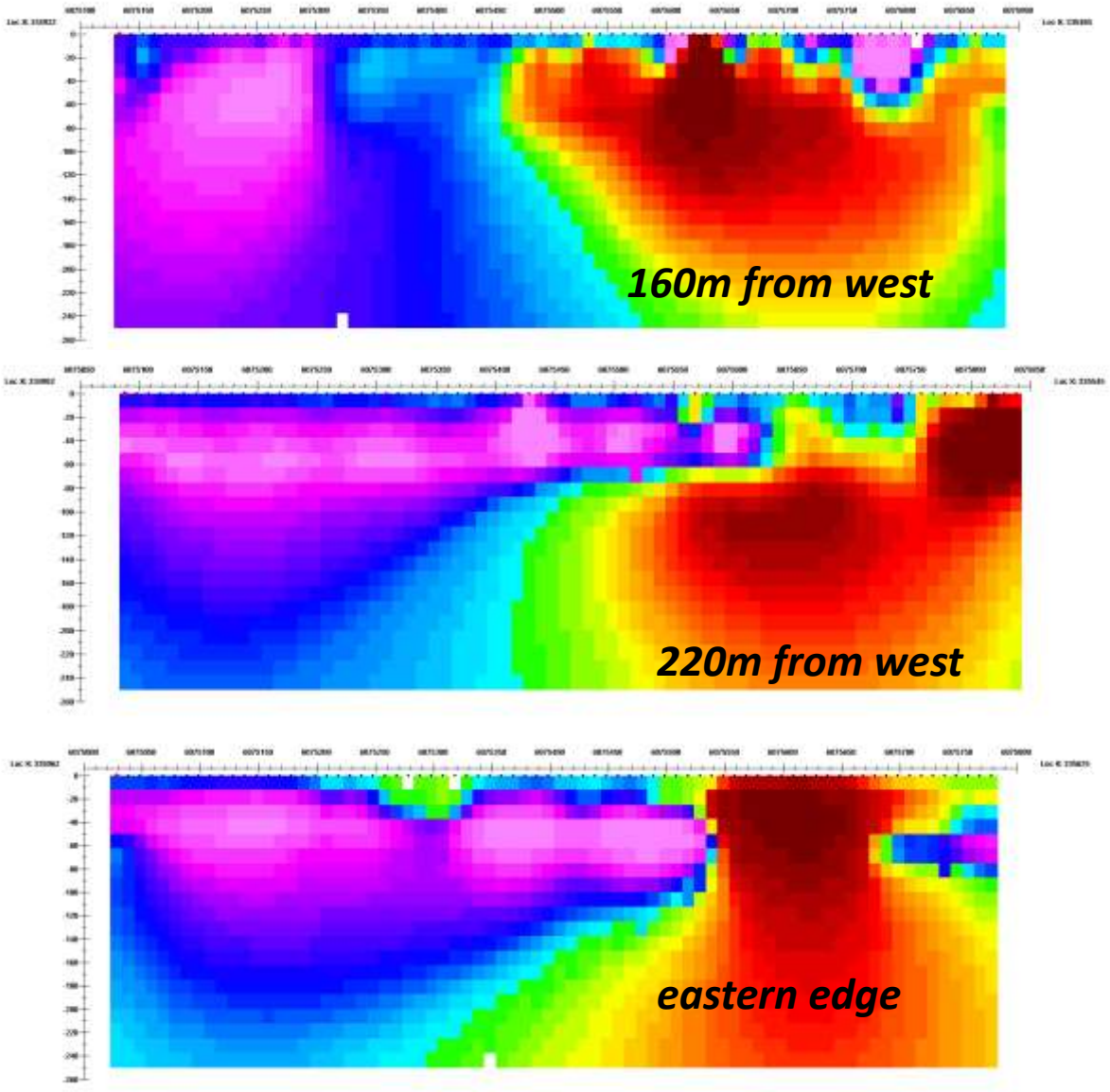

The magnetic structure continues east but is buried until the eastern edge of the grid. What is clear is that there is a magnetic boundary about 300m down grid but the structure appears to continue to the SE.

3D Inversions: 2D Cross Section slices parallel to strike

We now consider slices of the inversion perpendicular to strike starting from near the south end. We move along the strike from south to the distance indicated and then slice. In some figures, there is some interpolation to smooth the results. Colour ranges are consistent with earlier figures.

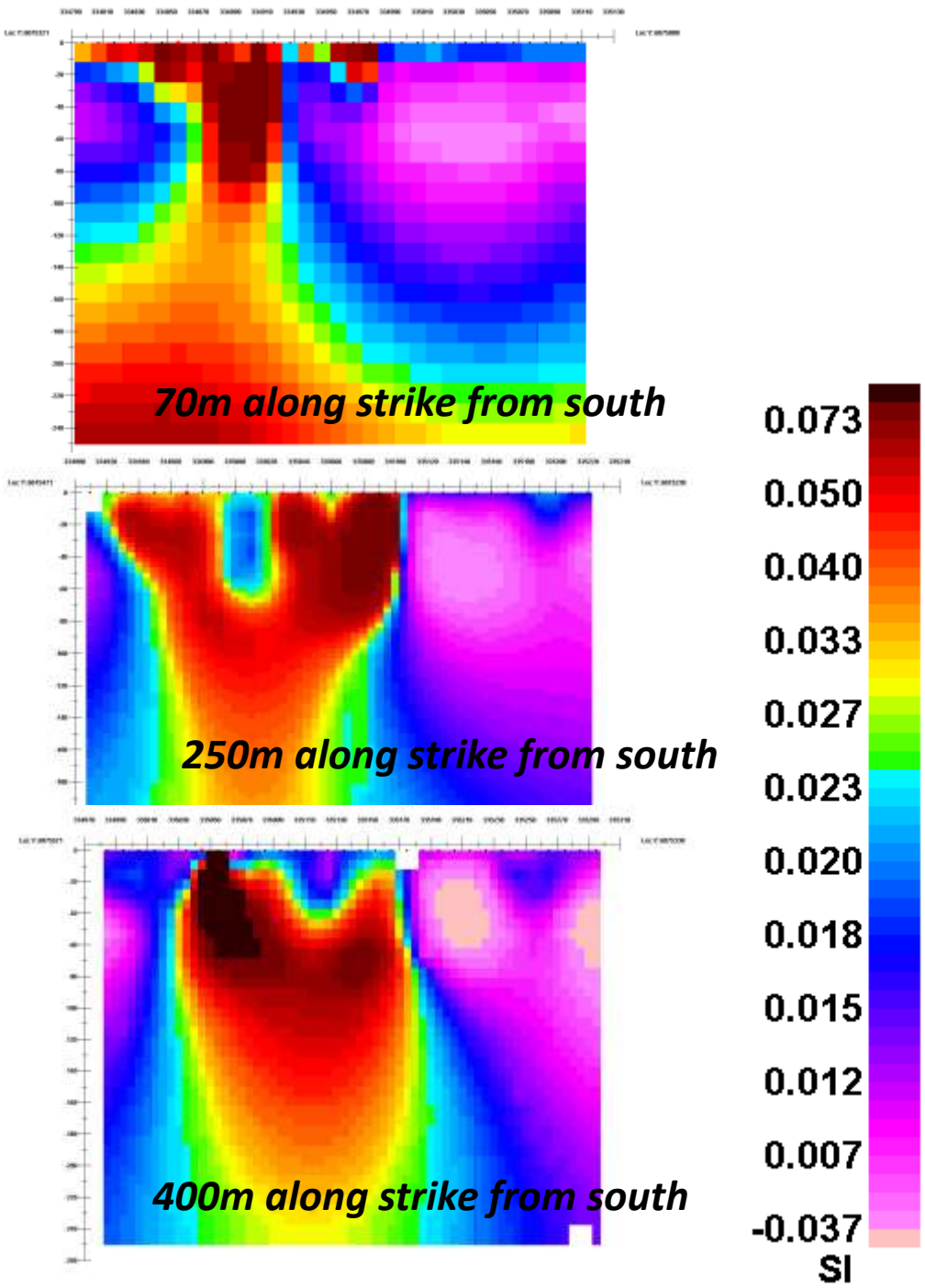

Figure 14: Inversion sections perpendicular to strike southern end

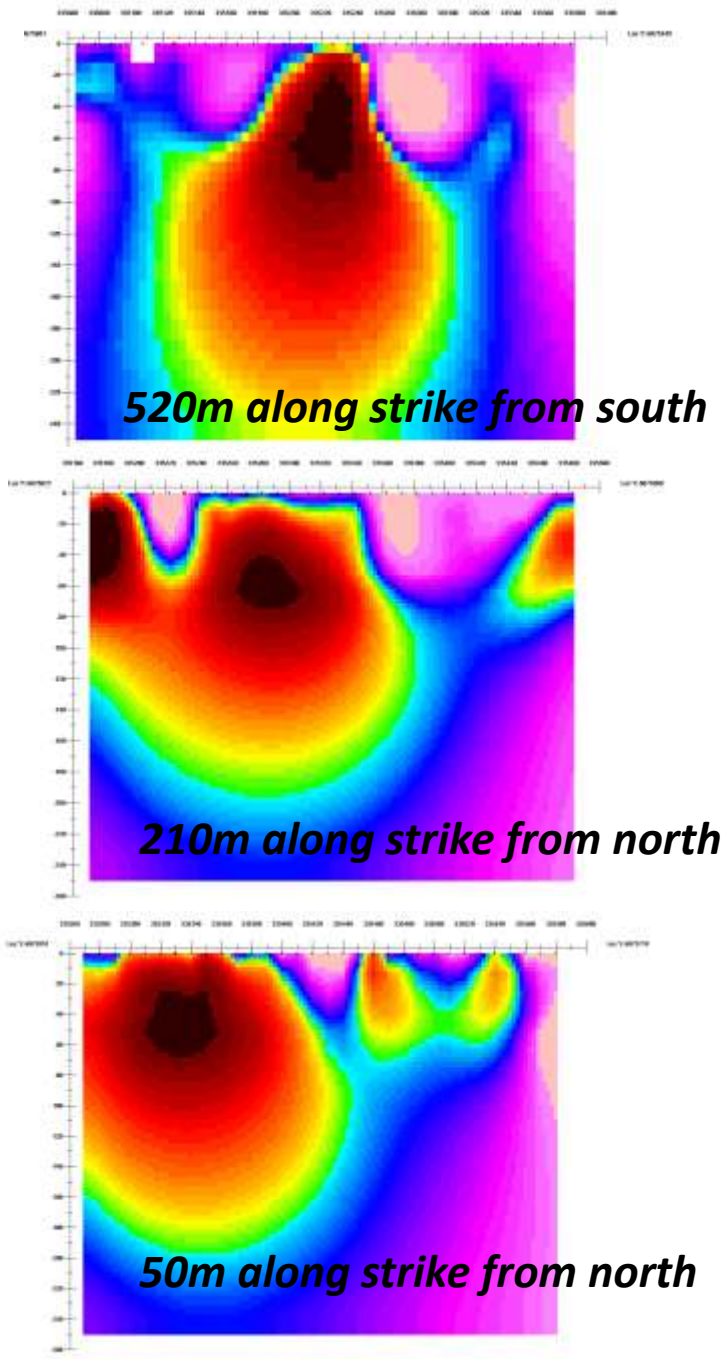

Figure 15: Inversion sections perpendicular to strike northern end

In the northern part of the grid, the magnetic data shows little indication of the shear structure. Whereas, in the south, the magnetic structure is entirely different and there is an EW boundary.

In Figure 16, we examine a depth slice of the inversion at a depth of 50m. This depth is such that it is not so dependent on the small scale features of the data.

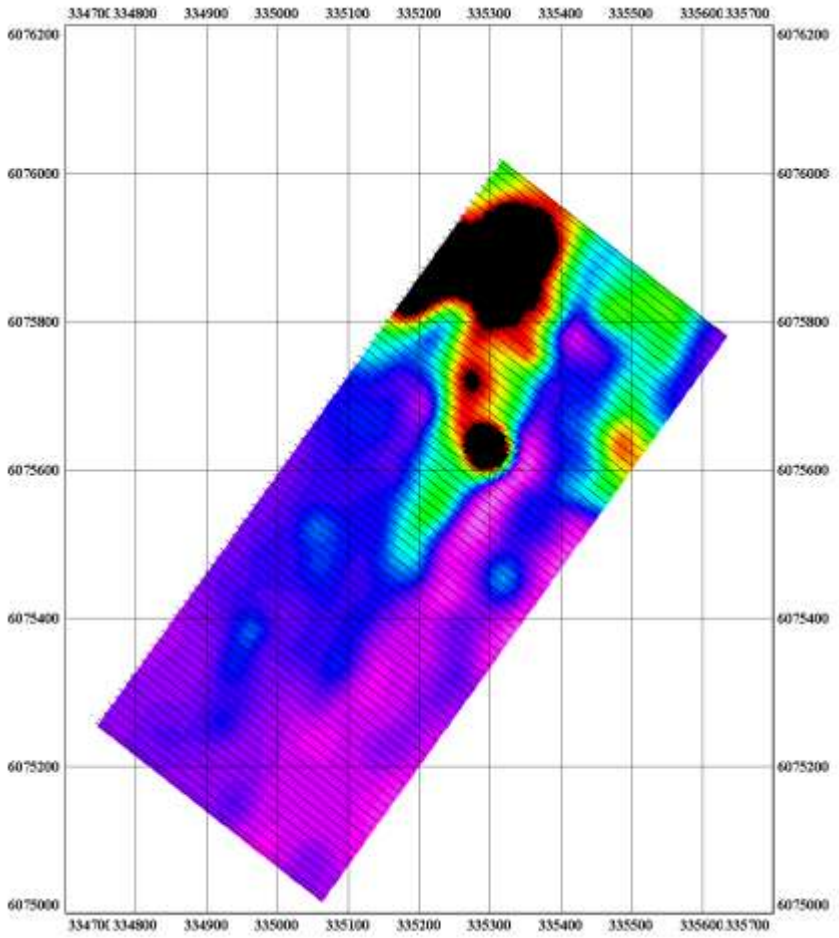

Figure 16: **Magnetic Inversion at depth of 50m**

Ground magnetic data in comparison to aeromagnetic data

The ground data is quite accurate data and importantly unfiltered for both the measured data and the base station data. This is quite different from the airborne data which is highly smoothed via filtering. We have gone back to the Geotech data and reprocessed as best as possible from the delivered data. Certain parameters were requested of Geotech to enable us to reprocess accurately but they were unwilling to provide this information.

The airborne data was IGRF corrected by us and then the 2010 to 2018 IGRF shift added to the data in order to enable direct comparison to the 2018 ground data. The EW survey lines of the main survey were combined with the SW to NE survey lines of the Albert's Lake survey. There is an IGRF variation which could affect integrating these surveys. The flight dates and details are not provided by Geotech in order to correct for IGRF variation over the entire period of airborne surveying. When, we requested these details, they did not respond. We would very

much like to have had the aeromagnetic data and base station data for the airborne data in order to process properly. It is important to note, that the base stations were far from the survey area. While, this is convenient for the surveying company, it does not allow for proper corrections of the data. By having a remote base station, one can do nothing but remove the smooth diurnal variation and nothing about removing ionospheric signals.

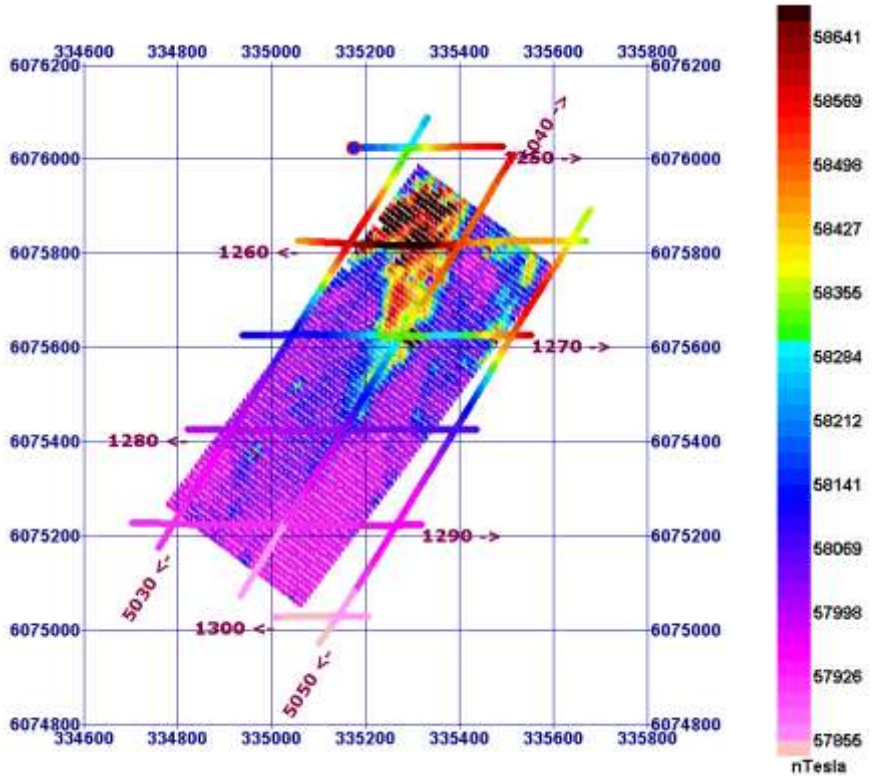

Figure 17: **Aeromagnetic data with ground data underlain**

Portions of 9 flight lines are utilized. The line labels are indicated in brown on the map (Fig 17). Data is represented by coloured dots along the lines. The legend for the airborne data is provided. A map of the gridded ground data is underlain. Amplitudes to colour are roughly the same but the range of the ground data is much higher than the airborne data. (57,855 to 58,659) compared to (57,450 to 68,985).While the general trends of the airborne data seem to agree with the ground data, there is very little detail in the airborne data which is surprising as the data was collected at an altitude of about 80m. We are unable to know exactly the altitude of the magnetic data. Details of the system and processing that would be required to precise position the height of the aeromagnetic data were some of the information that Geotech was unwilling to provide.

Here, we will focus on only a few features. The first feature is the strong high on the ground survey on Line200N mentioned previously. The ground data is contoured and underlain (Fig 18).

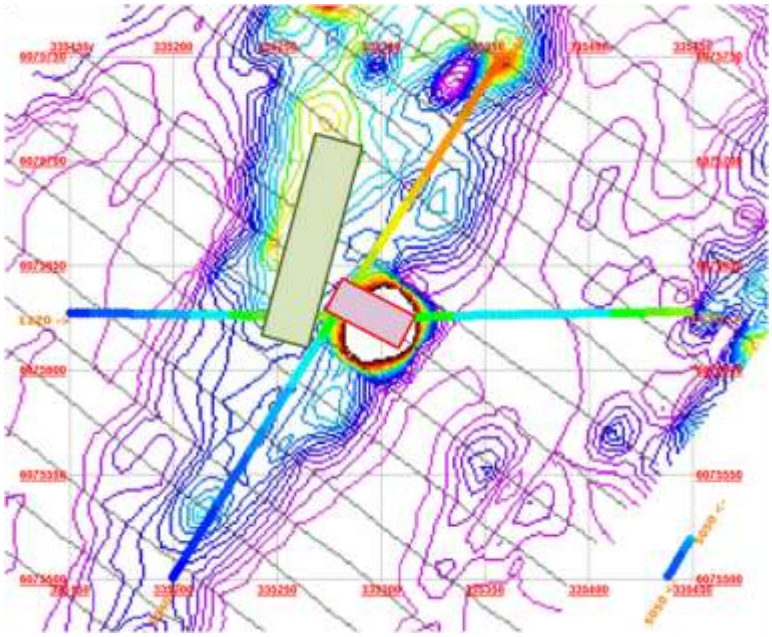

Figure 18: **Airborne magnetic data over strong high in ground data. Pink and green blocks are the surface representation of approximate 3D models of the ground response.**

The airborne data is displayed without gridding with the same amplitude scale as in the previous figure. There are at least 3 features to observe on this map. First, there is no strong high in the airborne data over the feature at (335300, 6075625) on L1270 which appears in the ground data even though the survey flew directly over this feature. The lesser high in the ground data at (335358, 6075750) does show in the airborne data on L5040 but there is a gradient to a moderate high on the airborne data shown south of this feature which does not appear on the ground data. Another significant feature is seen also on L1270 east of the previously mentioned high. Here the airborne data starts to increase easterly far before a more moderate increase begins in the ground data.

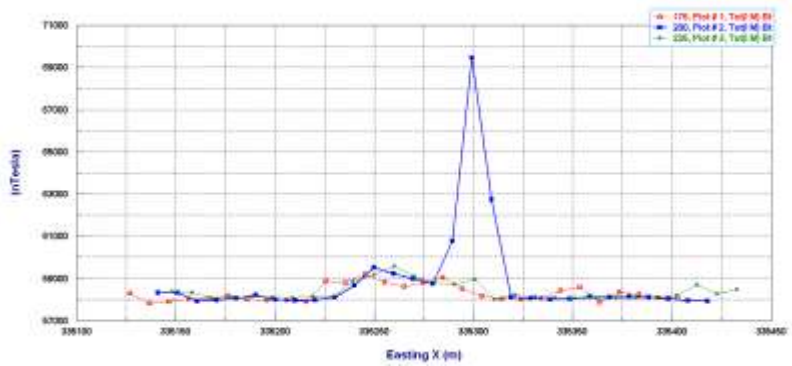

Figure 19: **Ground data on L175, 200 and 225N)**

The strong high in the ground data occurs only on L200N but does occur at 3 data points over at least 50m along the profile. Our modeling has determined that this is a very highly magnetic

feature dipping slightly NE about 35m in length and approximately 15m in width. There is not enough data coverage to separate out the thickness of the object but it seems to be essentially exposed.

For the ground data, we modeled the two (2) features shown in Figure 20 as pink and green rectangles. A modestly magnetic feature was used to simulate the response trending a few degrees east of North (light green), and a very strong magnetic structure dipping along L200N (pink). These represent the ground data in a gross sense for the 3 lines 175-225N as shown in the plot above. We now simulate the response of the models to the airborne altitudes.

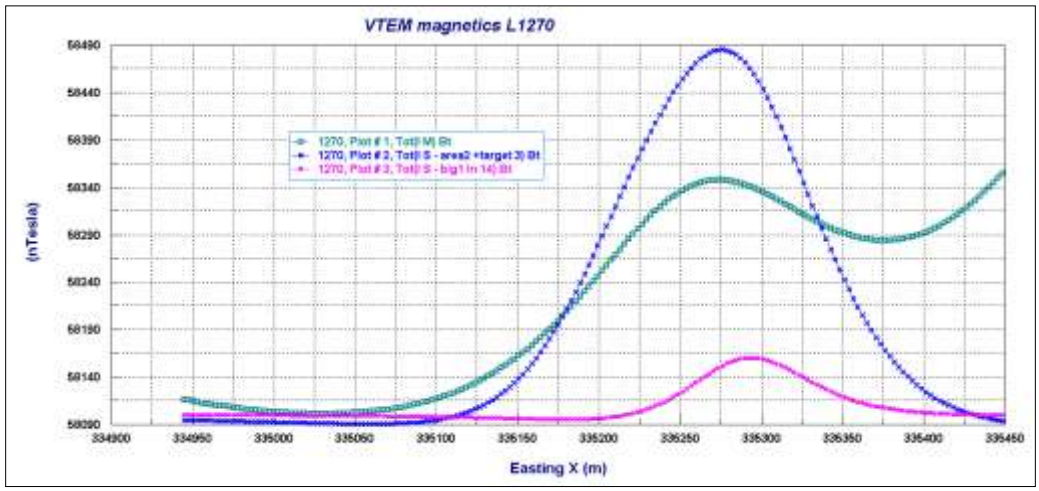

Figure 20: **Line 1270 aeromagnetic data versus simulated data to models**

In Figure 20, green is the data, while pink is the response at the altitude of the airborne data of the highly magnetic surficial target and blue is the combined response of the long approximately NS structure plus the highly magnetic target. The surficial target has a very smooth response at these altitudes and combined response is a little high. We have not attempted to include the magnetic feature to the east. These results are fairly consistent but not very satisfying still indicating a need to properly process the airborne data.

Upward continuation is a standard tool for such data to determine the response at a higher altitude. There is no theoretical proof for such processing but the method has proven reliable for several decades. Here, we have upward continued the ground data and presented it underneath contours of the aeromagnetic data (Fig 21). Data contours and underlain data are in the same data range.

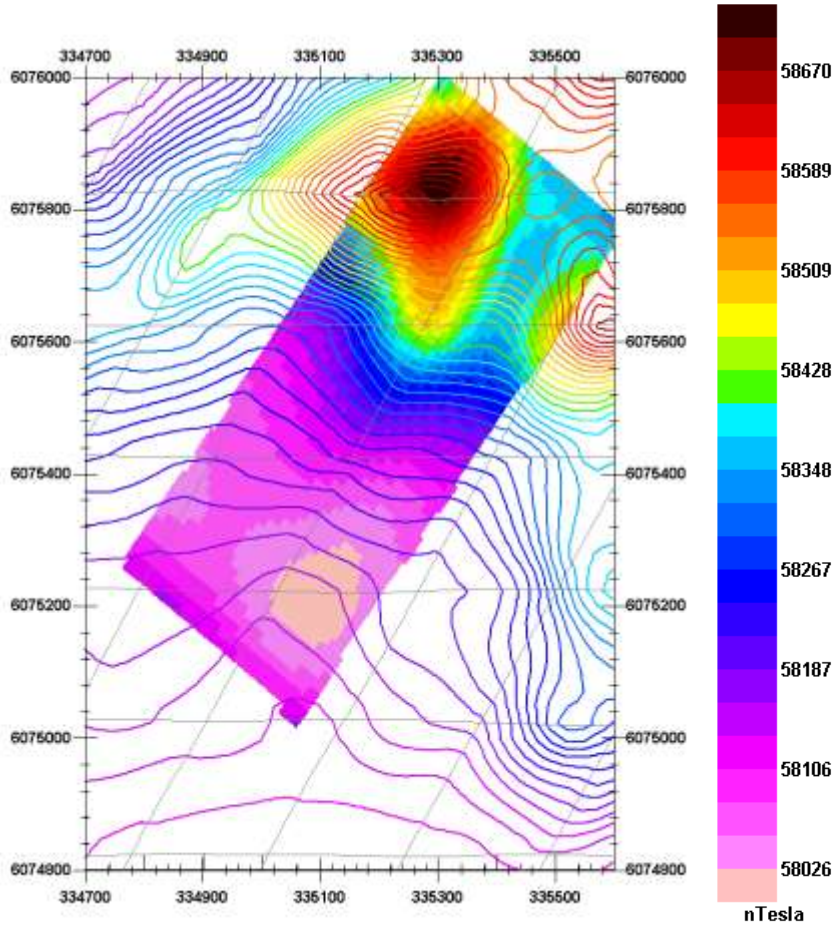

Figure 21: **Aeromagnetic data contoured with ground data upper continued to airborne altitudes contoured and underlain**

The comparison is somewhat satisfactory but two contradictions stand out. The airborne data over the NE part of the grid does not agree at all with the ground data. The amplitudes are too high and the low trending NE does not appear. The second aspect is the amplitudes and shapes at the south end of the grid.

We now show the analytic signal of the aeromagnetic data contoured with the ground data underlain (Fig 22). The analytic signal is the total response of the gradients of the field. This representation of the aeromagnetics does show more correlation with the ground data. The general high in the ground magnetics in the NW of the grid corresponds to a high in the analytic signal. The linear feature as marked in the ground data does appear in this representation of the aeromagnetics and the low trend as marked in the ground data appears as a low in the analytic signal.

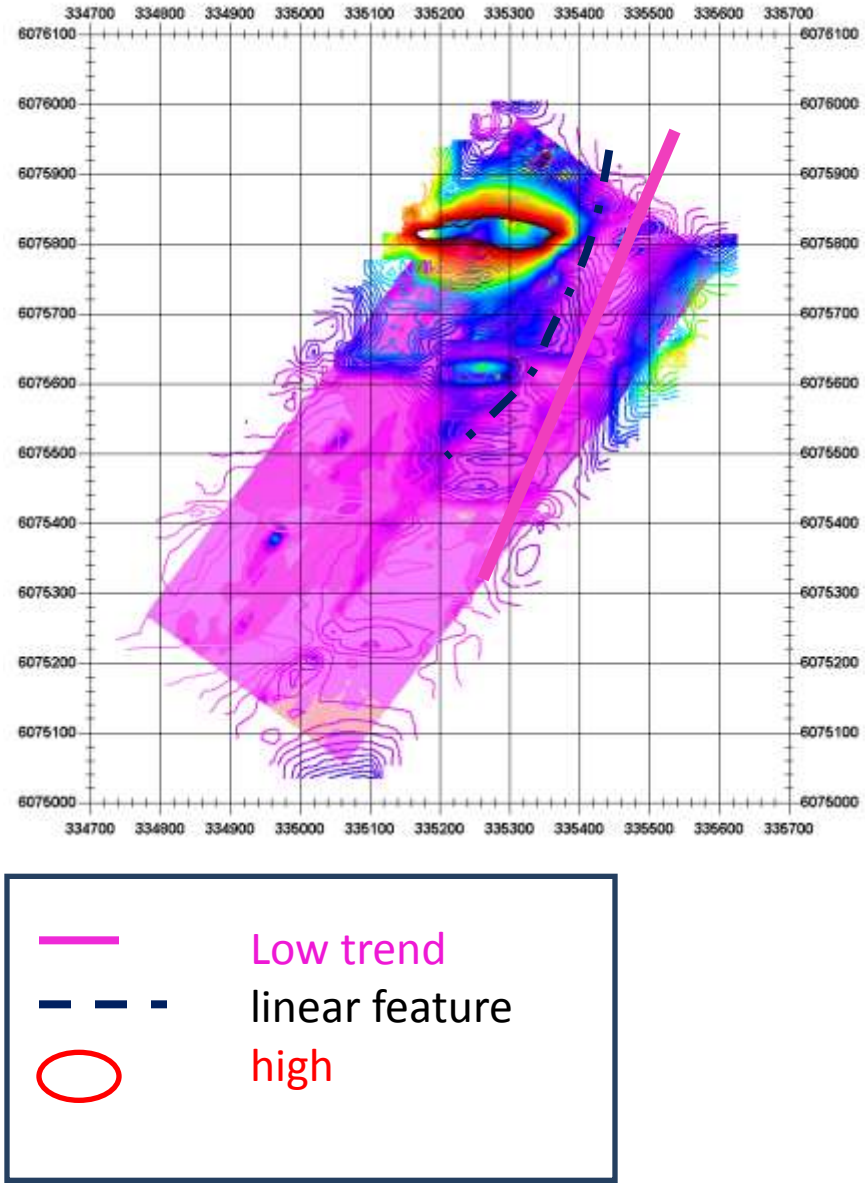

Figure 22: **Aeromagnetic data analytic signal contoured with ground mag underlain**

Ground data summary and recommendations

The ground data is of good quality and does indicate structure at shallow and intermediate depths. However, higher resolution data would likely be more useful in such geologic environments to better discriminate linear features. A walking magnetometer which would provide data at 1-2m intervals is common practice today and requires little more in the cost of data collection, processing and interpretation. Extending the grid to the north would help discriminate the magnetic high area in the NW of the grid.

Analyses and Preliminary Interpretation of 2018 Leo Lake VLF data

Summary

Survey

A combined VLF and magnetic survey was carried out in January, 2018 by Jason Sigfrid using a combined VLF and magnetics instrument (GSM-19) manufactured by GEM systems of Ontario.

VLF data was collected for 2 frequencies from 2 VLF transmitters at Seattle (NLK) and Cutler (NAA). The frequency for Cutler was 24 KHz and for Seattle 24.8Khz. 1073 distinct stations were measured on 37 lines with 29 stations per line. Data repeats were sufficiently similar to allow averaging. Nominal station spacing was 12.5m and nominal station spacing was 25m. GPS locations of grid stations were computed by interpolating GPS locations at the beginning and end of each line. Line labels were made from -400 in the south to 500 in the north.

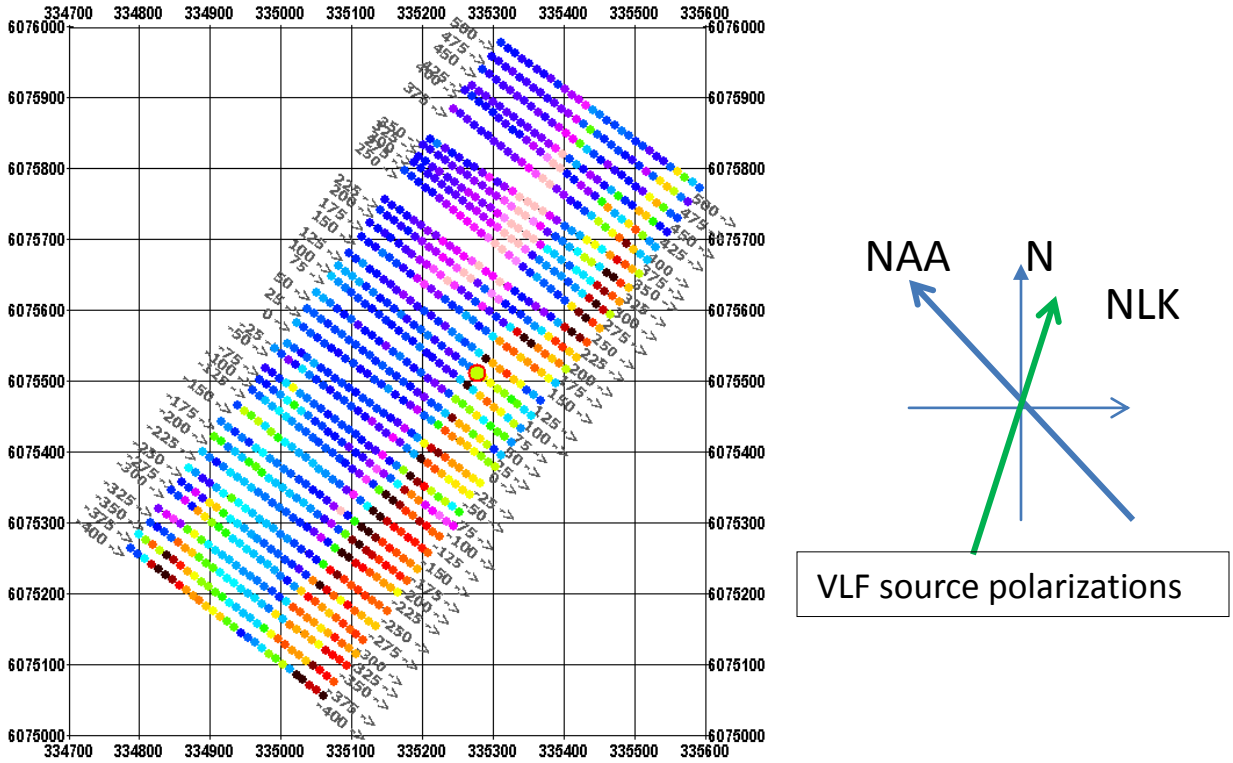

Figure 23: **VLF Survey with source polarizations**

Figure 23 shows the OP VLF data for the Seattle transmission. To the right is indicated the electric field polarization angles for the two VLF transmitters.

Data Quality:

A few repeats were made but these were very repeatable measurements which do imply that the signal strength was good and there was very little interference signals. The data appears to

be of good quality although this cannot be absolutely verified as so few repeats were taken. It is observed, however, that there is a reasonable consistency between the data collected due to the Cutler transmissions and those of the Seattle transmissions.

The survey line azimuths are approximately 53 degrees west of north on average. Assuming the survey lines are perpendicular to strike, the strike would be 37 degrees east of north. This is approximately the strike of the Albert's Lake fault as determined by Manitoba government geologists.

This geological strike is not optimal for the polarization azimuth of either VLF station. The optimal polarization angle for the VLF signal would be 37 degrees east of North. The Cutler polarization is 45 degrees west of north while the Seattle polarization is 10 degrees east of North. The Cutler polarization is almost the worst possible while the Seattle is therefore the best signal available. The North Dakota site could have been used.

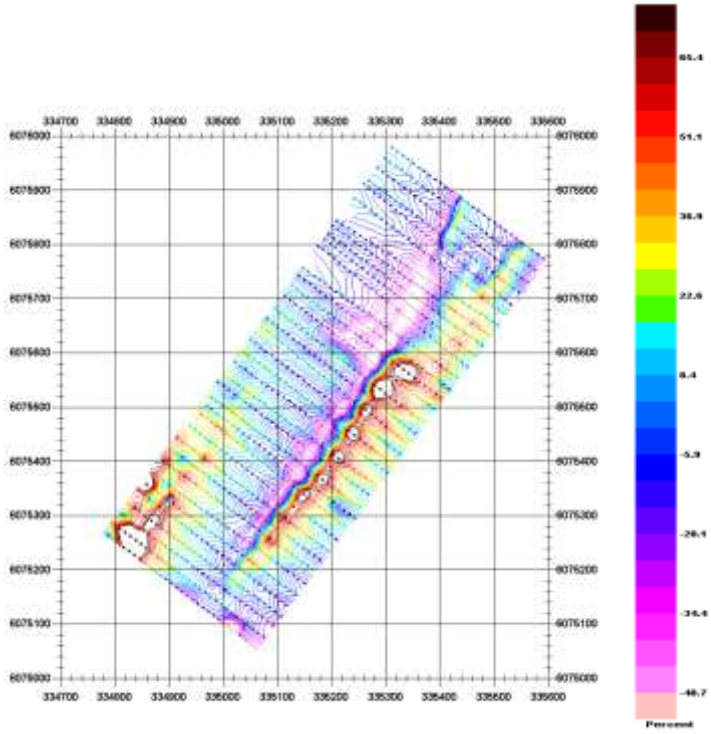

Figure 24: **InPhase Hz (IP) Seattle in %**

Figure 24 is contours of the In Phase (IP) due to Seattle while figure 24 is the IP due to Cutler. The Seattle signal should be the best signal to illuminate a SW-NE structure. However, despite Cutler being theoretically almost the worst possible polarization, there is close correlations between the data due to the two transmitters.

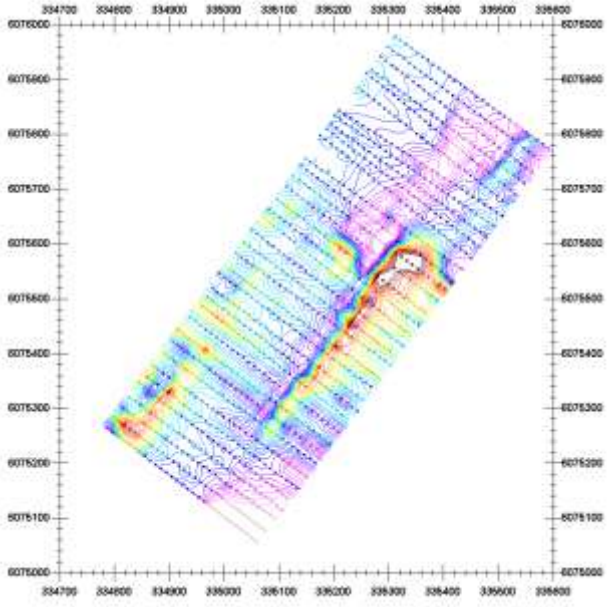

Figure 25 InPhase Hz (IP) Cutler in %

VLF Discussion:

The Seattle data generally shows 3 features. First (Fig 24), there is a clear shallow vertical cross-over feature (CO1) in the IP across the central area of the survey. The strike of this response is very comparable to the strike of the Albert's Lake Shear as on the government map but the feature is offset by the mapped shear by about 80m. To the north, the response opens and the cross over is broader implying a deeper structure (CO2). As the survey lines are too short to cover the eastern part of this response, the dip of this target may not be able to be evaluated. There is a correlation with the widening of this crossover with the location of the small lake on the grid. There is an additional response in the SW but the nature of this anomaly is not obvious just by viewing the gridded data.

In the contoured view shown below (Fig 26), there is indicated a significant problem with the data. The response on the main feature is stronger over this feature along lines which were surveyed in an easterly direction as opposed to neighboring lines surveyed in a westerly direction. The surveyor has assumed that the instrument perfectly corrects for any issue of instrument tilt which apparently it does not. J. Sigfrid and R.Groom are presently carrying out tests to evaluate these issues.

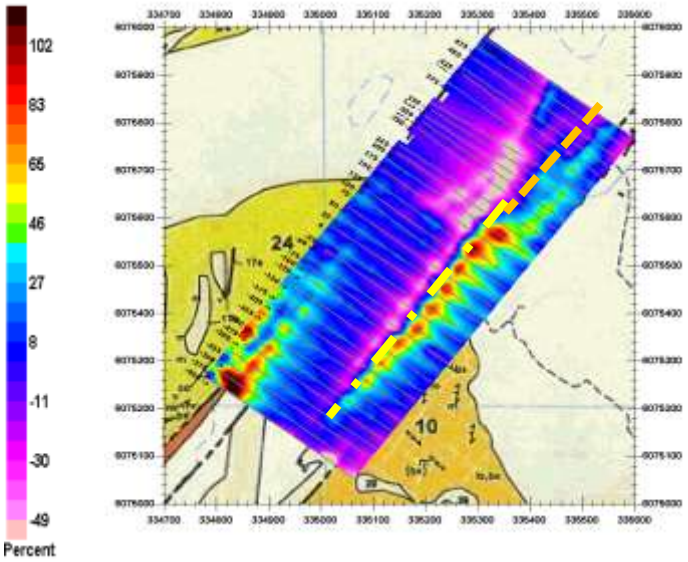

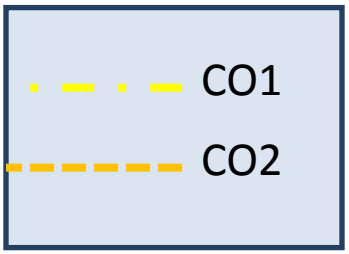

Figure 26 InPhase Hz (IP) Seattle contoured Geology map underlain

While, generally, the 3 main features remain in the out-of-phase (OP) or quadrature response (Fig 27, it is evident that the OP response is significantly smaller that the IP at least in the 2 main features. This would indicate a more conducting feature or excitation primarily by the electric field of the source.

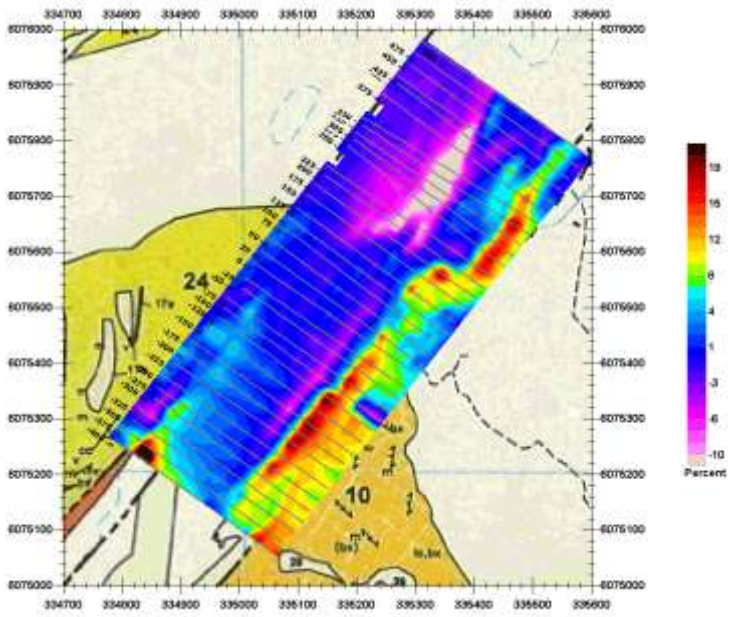

Figure 27 Out of Phase Hz (OP) Seattle contoured

VLF Data Levelling

Below (Fig 28), we plot the IP response for Seattle along 6 lines across the main C01 feature.

The 3 easterly lines (-175,-125 and -75) all have higher positive peaks and lower negative peaks than the 3 westerly lines. The crossover of the easterly lines is approximately 25% while that of the westerly lines is about 0% which is more what would be expected. In the OP phase data, this alternating response is still evident but not quite so clearly.

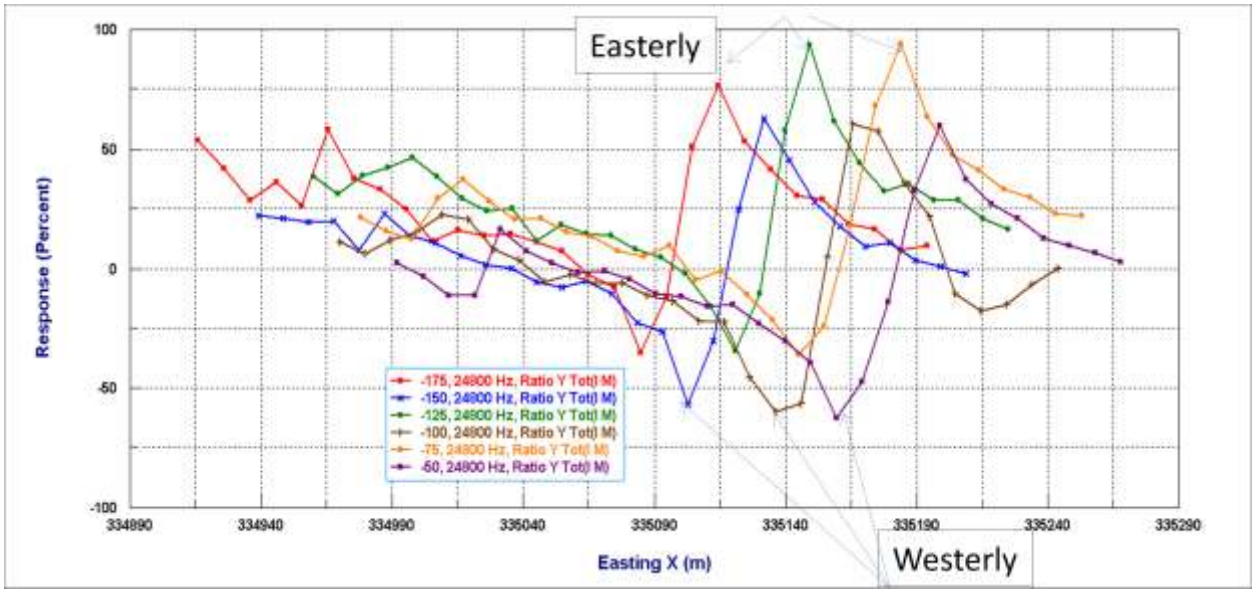

Figure 28 –Response shift **IP Seattle** across C91 – 6 lines

VLF Data Analyses

Below, we plot (Fig 29) the IP response and OP response for the Seattle data on 2 lines over the main linear feature (OC1). Data for lines -175 south (R,P) and -75 (B,GB) south are shown. The IP response is very sharp and well above the background noise. Peak to peak width is between 35-40 m and there appears little evidence of dip. The OP responses are much smaller and although far less clear than the IP, do maintain something of a crossover. Both lines are towards the south of the feature.

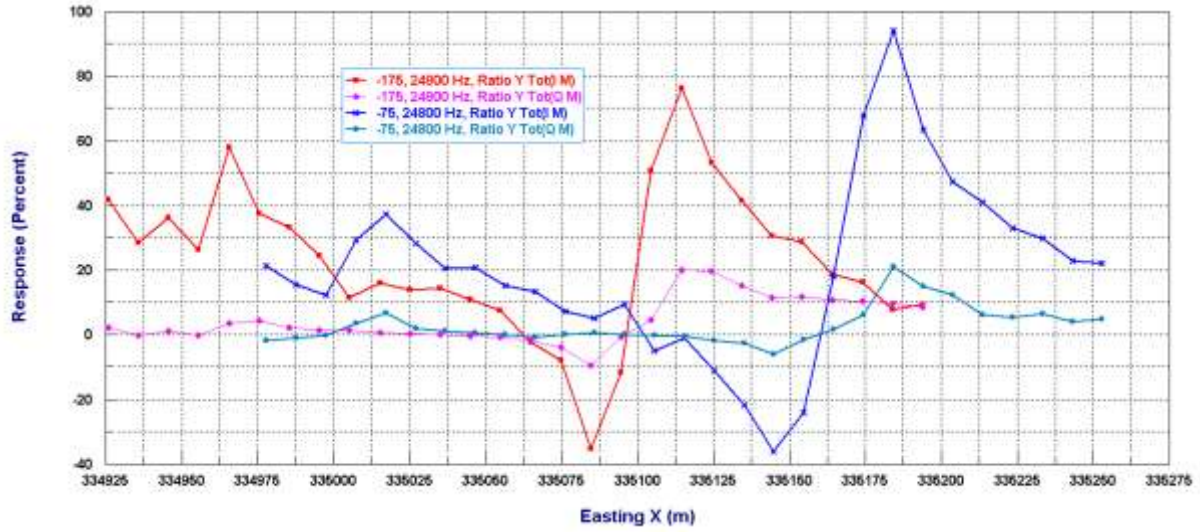

Figure 29 – InPhase/Out-of-Phase Hz (IP/OP) Seattle across C01 – 2lines (-175,-75)

Below, we plot (Fig 30) the IP response and OP response for the Seattle data on 2 lines over the northern feature (OC2). Data for lines 325 north (R,P) and 350 north (B,GB) are shown. The IP response is now broader but well above the background noise. The peak to peak width is now between 75-85 m which indicates a deeper structure. The OP responses are still much smaller and now far less clear. The problems with correct level may mean it will be hard to determine the dip.

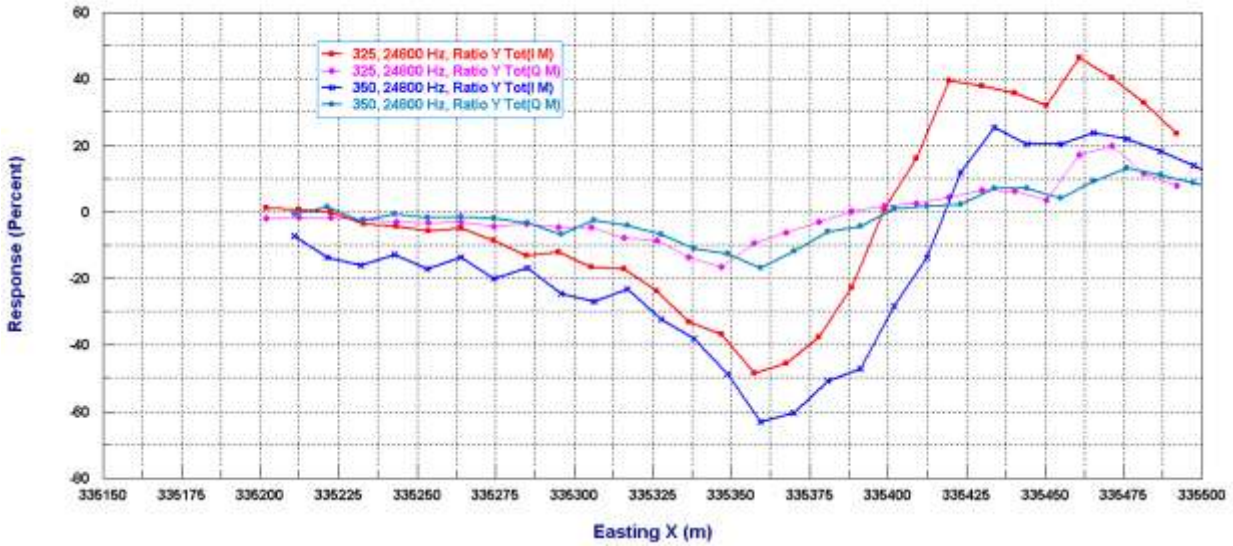

Figure 30 – **InPhase/Out-of-Phase Hz (IP/OP) Seattle across C01 – 2lines (-175,-75)**

Below, we plot (Fig 31) the IP response and OP response for the Cutler data on 2 lines over the main linear feature (OC1). Data for lines -125 south (R,P) and -100 (B,GB) south are shown. What is most striking is that the quadrature is no longer much smaller than the IP? The 2 lines are surveyed in opposite directions but the peaks are almost the same. The peak to peak width is less than fro Cutler and most noticeably, the responses are much smaller than the Seattle data and no so clearly above the noise.

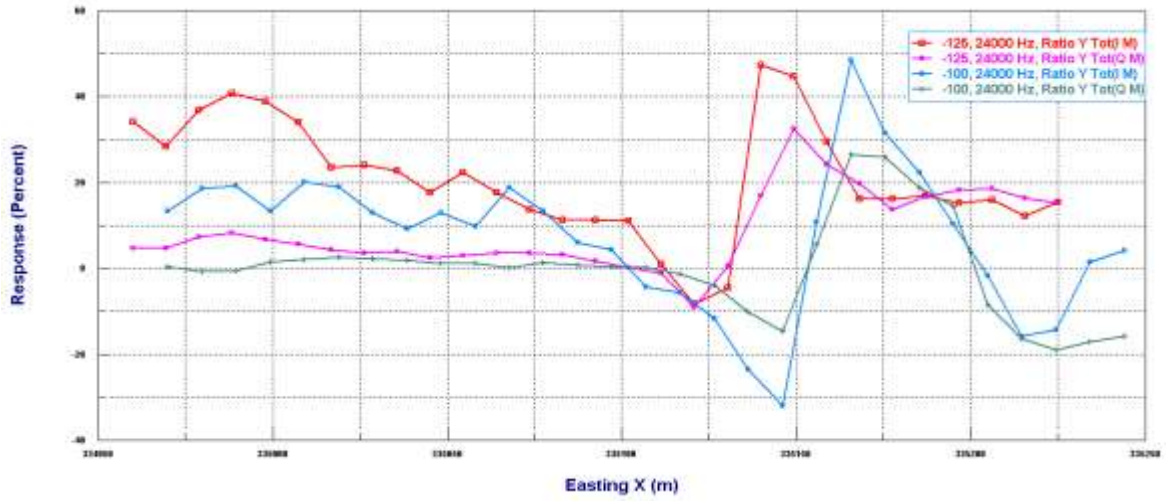

Figure 31 – InPhase/Out-of-Phase Hz (IP/OP) Cutler across C01 – 2lines (-125,-100)

VLF Data Modeling

Main Concepts

Many years ago much was written about the nature of the VLF response. However, in recent decades this topic has not drawn much interest. Many concepts, accepted by geophysicists, concerning the VLF response are not in fact true. Modern day modeling techniques help us to study this response more analytically. Below is a short summary of the basic concepts concerning the VLF response. More information is provided in Appendix A.

1. The source field which has propagated from the VLF transmitter is horizontal.

This concept is not strictly correct. The VLF transmitter is a vertical radio transmitter and radiates the EM field just as in the past for standard radio transmissions. To reach our survey site, it must propagate like a wave in the air with little loss and this it does as the fields travel through the air. The fields that enter the ground do not reach us as their strength is loss through inductive heating. As the waves reach our survey site, the fields change their orientation due to the impedance of the ground. Vertical electric field from the source rotates so that it is a horizontal field with its polarization directly in line with the VLF transmitter. The magnetic fields which travel with the electric field also rotate to be horizontal at the surface and below the surface of the ground. It is important to understand that in order to interpret the data either via modeling and physical intuition, the ground impedance must be sufficiently low to cause the source fields to be horizontal. If there are still partially vertical, we cannot know how vertical and we are lost. This is the main obstacle to collecting VLF in an airborne system.

2. The VLF response is an inductive response caused by the horizontal magnetic source fields.

This concept is also not strictly correct. We know this because the magnetotelluric fields and in particular the tippers are very analogous to the VLF fields.

We know from MT, that the electric field of the source can also play a role and not just the magnetic fields from the source. As it is very difficult, if not impossible to utilize VLF except in very resistive environments, we will limit our discussions to such an environment. A conductor in the ground can pick up the electric field just like a traditional radio antenna and this produces a current in the conductor which then radiates a magnetic field. Of course, the traditionally understood VLF response as due to induction from the horizontal source fields is also present. Which is more prominent depends upon the characteristics of the conductor and is governed by standard EM concepts. But, simply put, if the conductor does not have a good depth extent and has a long strike length, them the excitation from the electric field will dominate. To maximize the inductive response which is more capable of resolving the conductance of the conductor, one needs to try to have the structure following the polarization of the source electric field.

3. The VLF response is governed only by the burial depth, the conductance, the depth extent, dip and strike angles and strike length.

This statement omits one important factor and that is the resistivity of the host. The resistivity of the host and in particular the resistivity and thickness of any cover to the resistive

rocks plays 2 roles in the response. First, of course, it governs how much source signal excites the anomaly and how much secondary signal reaches the Rx coils on the surface. But, it also governs the phase relation of the source fields and thus directly impacts the relative amplitudes of the IP and OP VLF components. This is most critical if the electric source field plays a critical role.

3D Modeling

First, we will consider the main feature which we have termed CO1 (crossover 1). Below, we plot the IP and OP field on Line 50S (Fig 32). This line is chosen as a first example, as the crossover is near zero. That is, if we take the difference of the positive peak and the negative peak, we get approximately zero which we expect from a non-dipping structure. This is true for only 50% of the lines crossing 50S due to the likelihood of a tilt problem in the data.

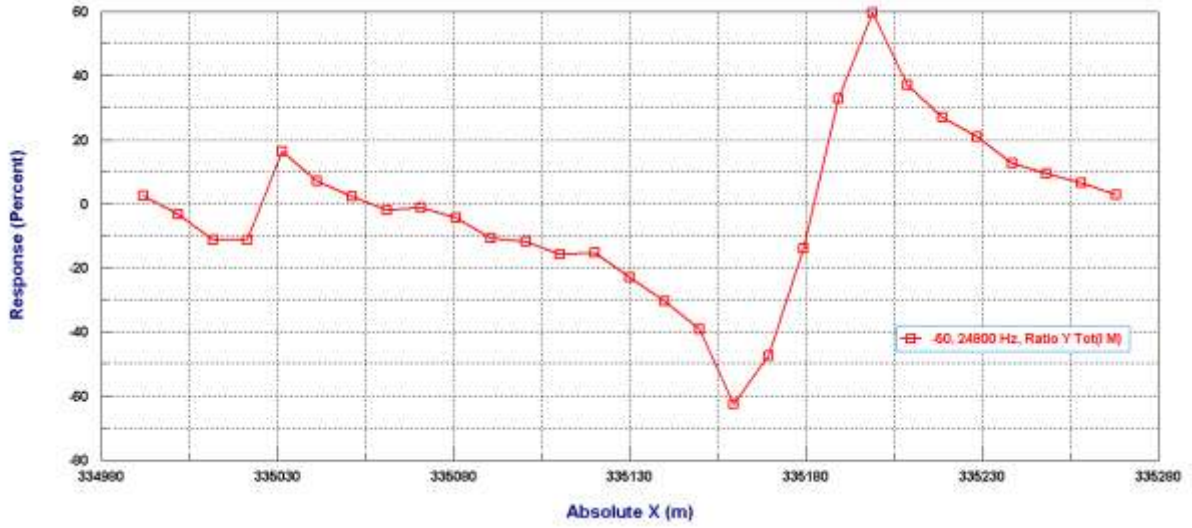

Figure 32 – InPhase Hz (IP) Seattle across C01 – Line 50S)

- **fall-off (tails) from the peak is spatially quick – shallow depth extent or short strike**
- **crossover symmetrical - non-dipping**
- **distance from peak to peak is 50m**

Conclusion 1: The depth extent is relatively small. The anomaly appears to be contiguous with a strike length of about 400m. Therefore, we conclude the depth extent must be shallow.
Conclusion 2: Depth to top is relatively shallow but not extremely shallow

OC1 model: This model fits the IP data quite well for the lines which were surveyed in a westerly direction. However, for the alternate lines surveyed in an easterly direction, there is an evident shift in the data.

Model LN15:
- **Depth to top: 5m**
- **Depth extent: 20m**
- **Strike angle: 37 degrees east of north**
- **Strike length: 400m**
- **Conductance: 25 Siemens**

In Figure 33, we show the data along an easterly surveyed line (L25S) versus the synthetic data from the model. Here it is evident that there is a positive shift in the data. The response as we move away from the conductor does not approach zero but rather something close to 10 or 15%. The data compared to the model is shifted and the crossover value is not zero. If the instrument were tilted so that the vertical measurement collected part of the horizontal field then this would be what might be expected. This may provide a clue as to how to correct the data.

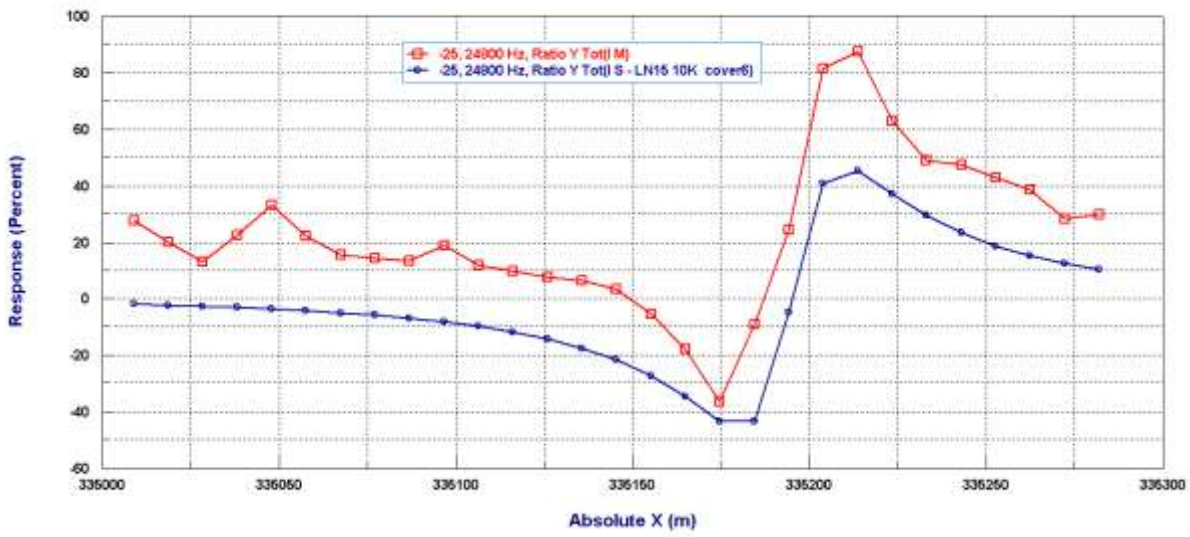

Figure 33 – InPhase Hz (IP) Seattle across C01 – Line 25S – data plus model

OC1 model: Out-of-Phase (OP) or quadrature response (Fig 34). The peak positive response for the OP along this feature is in the range of 20% while the negative peak is lower in the range of -15%. The problem that we have with the quadrature is that we know there can be an error in the IP of about 10-15% and thus we might expect a fairly significant OP error.

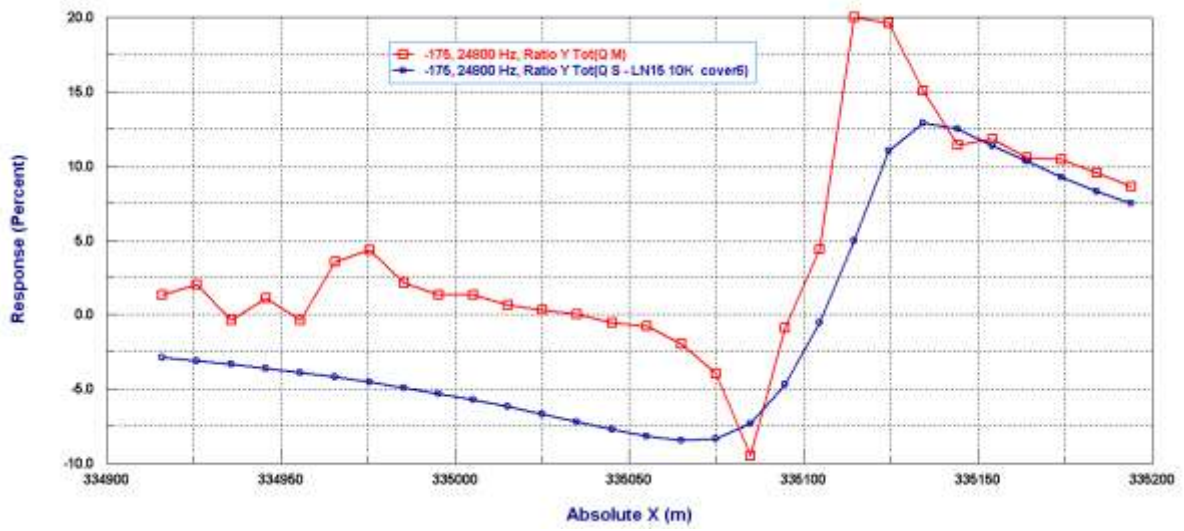

Figure 34 – Out of Phase (IP) Seattle across C01 – Line 175S – data plus model

OC2 model: In the north of the survey, there is another identifiable feature marked below (Figure 35). Here, the peak to peak width is much larger than for the southern feature at about 120m implying a deeper structure. It might be attractive to interpret this as 2 features but we are relatively certain that this is primarily one feature.

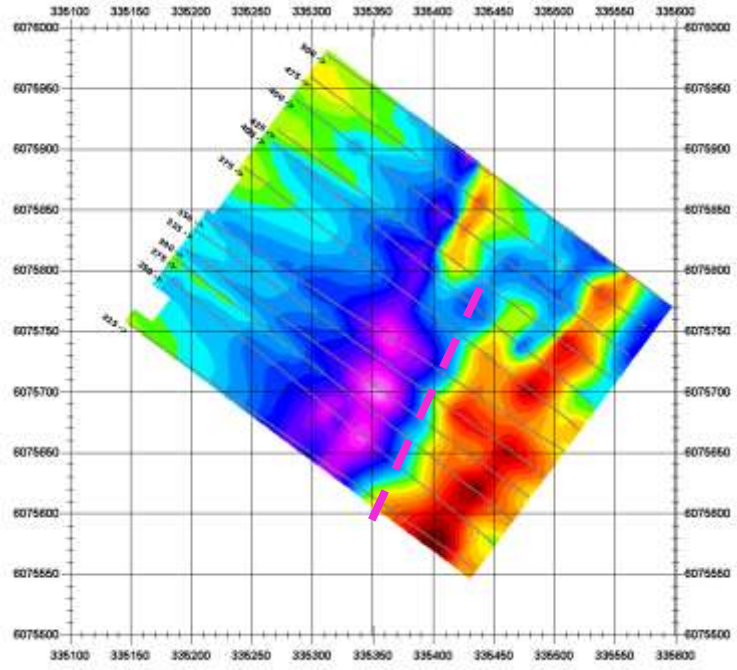

Figure 35 – InPhase (IP) Seattle across C02– L225-500N

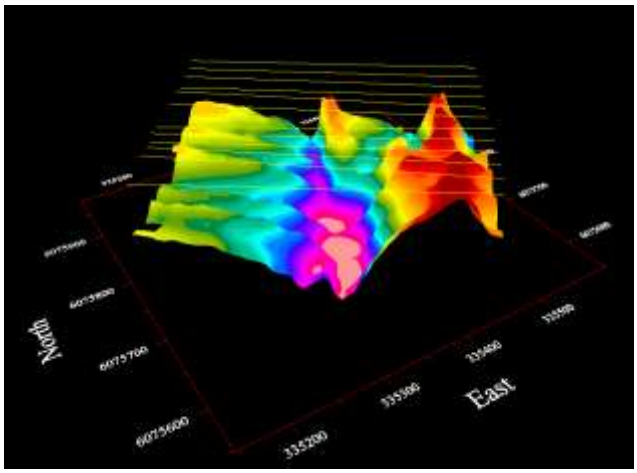

Figure 36– The IP response represented as a surface.

The viewing of the response over OC2 as a surface (Fig 36) makes it easier to view it as a single structure. The orange spike in the center north is another feature but difficult to analyze with the limited data. Here, the peak to peak width is much larger than for the southern feature at about 120m implying a deeper structure. Again, we have a shift between the westerly line (L250,L300) and the easterly lines (L275) (Fig 37).

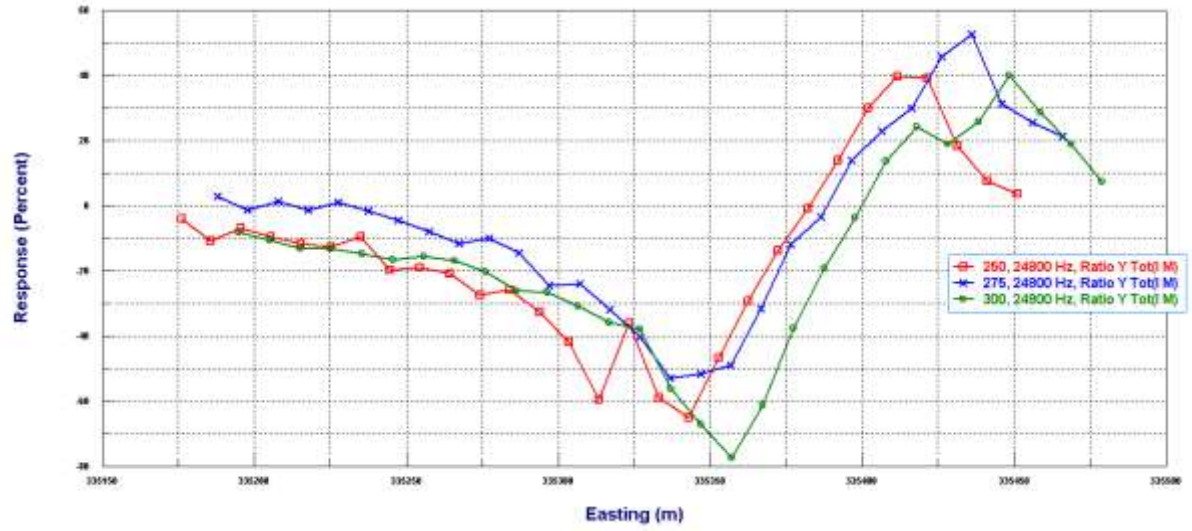

Figure 37 – InPhase (IP) Seattle across C02 L250-L300

OC2 model: It has been difficult to find a satisfactory model. Possibly with more work, a better model could be determined. But, to date, this is our best models (Fig 38, 39). Here, we have computed various versions of the best model to try to determine the data's sensitivity to such things as depth of burial, thickness, conductivity, strike length.

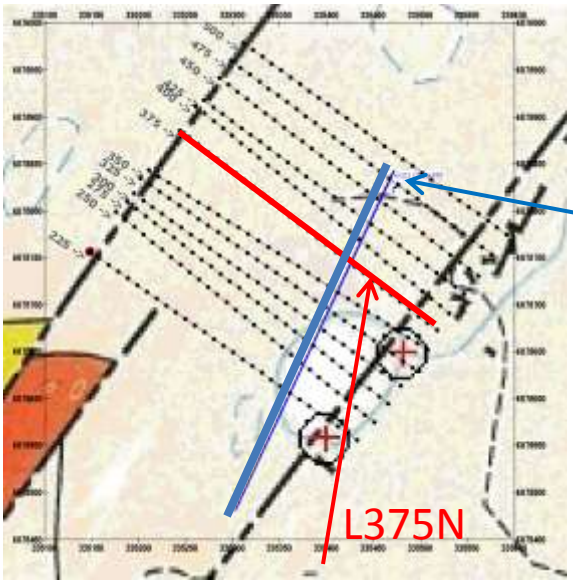

Model OC2 7:
- **Depth to top: 20m**
- **Depth extent: 15m**
- **Strike angle: 25 degrees east of north**
- **Strike length: 400m**
- **Conductance: 1-100 Siemens**

Figure 38 – Model OC2-7: L375

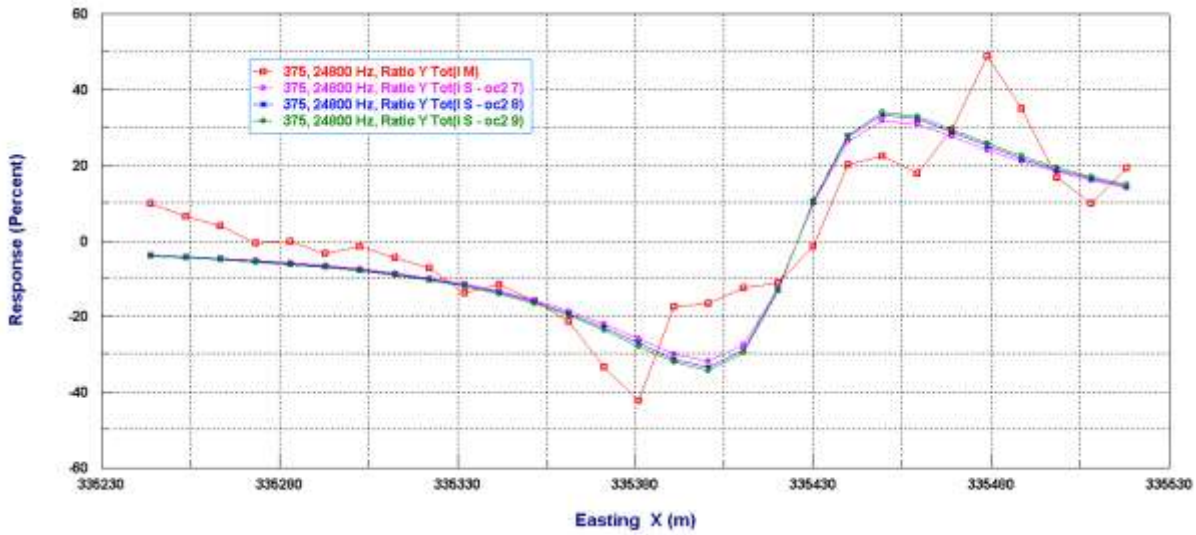

Figure 39 – InPhase Hz (IP) Seattle across CO2, L375

OC2 model: Three models are presented in this (Fig 40) and the previous slide. From our modeling, the conductor cannot be close to surface but must be buried in order to derive this peak to peak width. The 3 models vary in thickness and conductivity from 2 to 5m thickness and from 2 to 100 S/m. Increasing conductivity, thickness and depth extent has little impact on the response. But, we are unsatisfied as the peak to peak width is not sufficient to match the data. But, increasing the depth of burial produces a model with cannot reach the amplitude of these responses (Fig 40, 41).

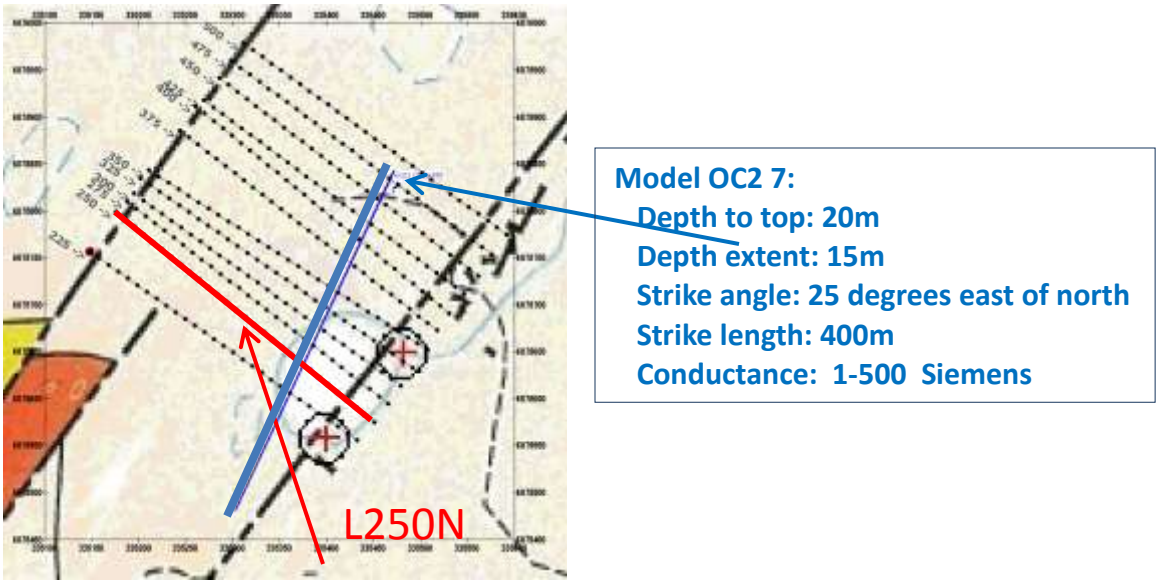

Figure 40a –C02 – Line 250N) with model OC2-7

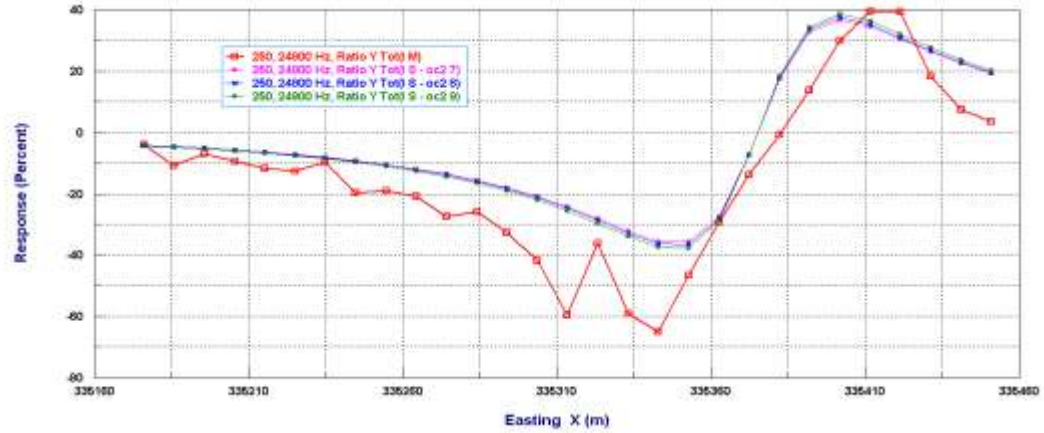

Figure 40b – InPhase (IP) Seattle across C02 – Line 250SN

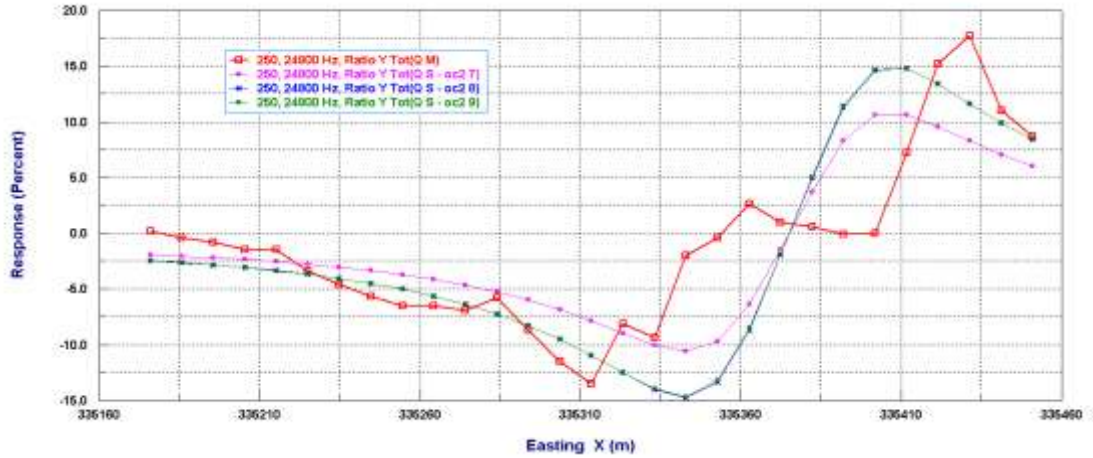

Figure 41 – Out of Phase (OP) Seattle across C02 – Line 250N

OC2 model: The quadrature responses are relatively small and only slightly above noise level. The modeled OP response does agree within noise levels with the data. For the OP component, the conductance of the structure does have an impact on the simulated response. However, it is not as yet clear, how to utilize this information.

VLF summary and recommendations

The VLF data is of good quality. However, the issue discussed of the feature seemingly shifted depending on direction of surveying should be resolved. This would likely require a calibration study of the VLF system.

Additionally, while we do detect features responding to the VLF signal, we do not know the reason for the responses and thus interpretation of the structures is virtually impossible. Examination of borehole logs for drillholes intersection the southern structure (OC1) might be useful to determine the reasons for the VLF responses and thus allow better structural discrimination both for this survey and for further VLF surveys.

Comparison of Ground EM to airborne EM data – VLF vs VTEM

As VLF responses can be due to the primary electric field responses, such responses can be due to very slight variations in resistivity. The source electric field will produce anomalous charges just as in a resistivity survey and even relatively small resistivity variations can be determined. Our modeling in the previous section appeared to indicate that the conductivity of the structures had little effect on the data.

However, airborne TEM and in particular VTEM has often been used to delineate some shallow structure. Thus, an obvious question is whether the VTEM "sees" the VLF structures. We must remember that the VTEM data in this environment is primarily due to excitation by the magnetic field from the transmitter.

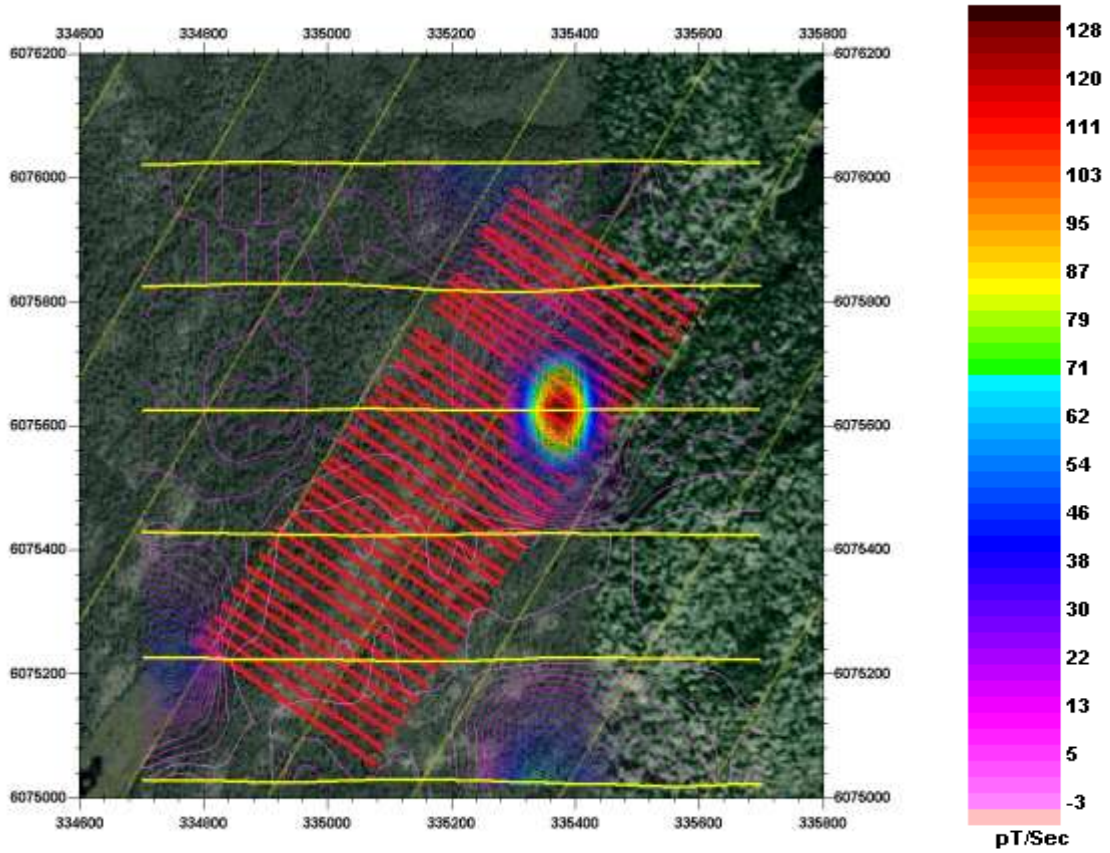

Figure 42 – VTEM early time with satellite underlay

Channel 3 of the VTEM Hz is contoured using only the data from the EW flights as the SW-NE flights are parallel to our structures (Fig 42). Earlier channels are not reliable. The main feature is the pond or small lake within the VLF grid. The response to the SE is related to the materials on the surface around Leo Lake. That response to the NW appears also to be an edge response from a surficial feature.

The VTEM instrument flies only about 40m above the surface. Thus, why the linear VLF features are not evident in the VTEM data is not clear at this point. As there is significant cover material in the area which is conductive and the VLF data shows that such cover is present most everywhere, then the VLF structures would appear as current channelling responses in the VTEM data. However, possibly the response of the cover is lost in the ambiguity of the early channel data.

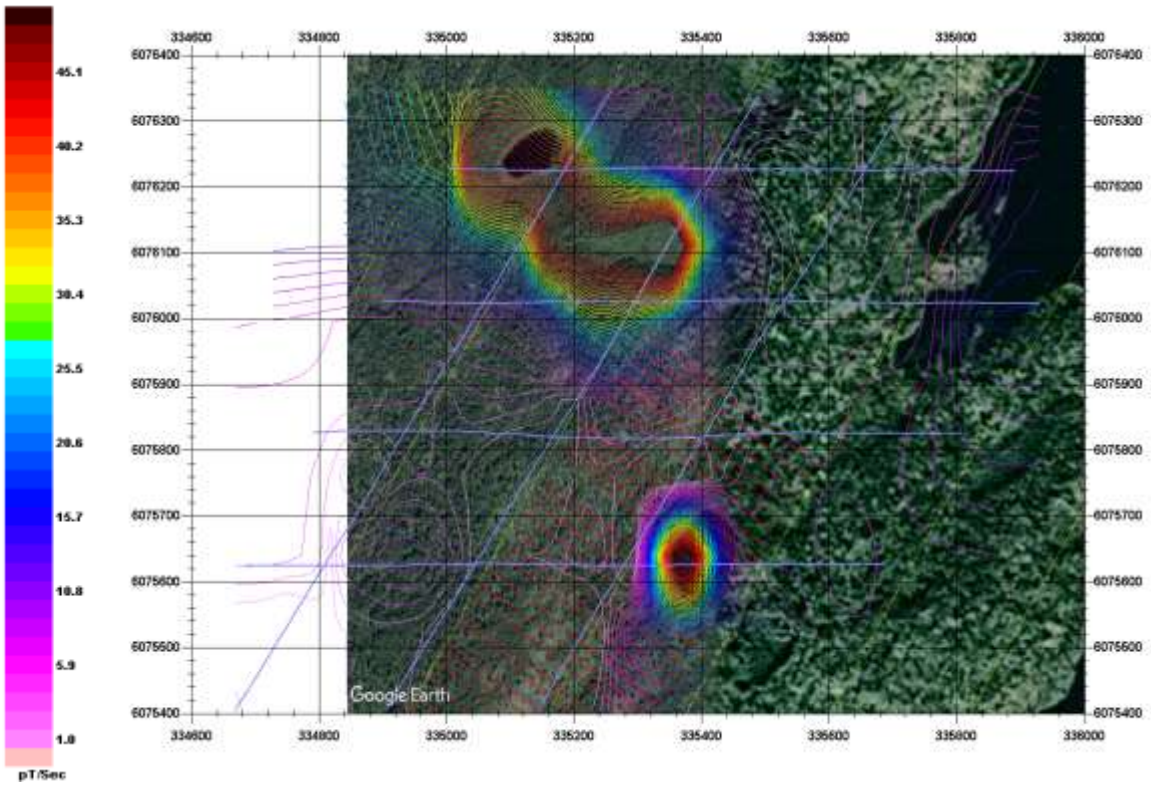

Figure 43 – VTEM Ch4– EW and NE-SW flights

Channel 4 is contoured (Fig 43). Mostly there is no ground response in early time except over the anomalies shown below. Both of these features appear associated with a ground feature as shown on the satellite map (Fig 43 and Fig 44). Flight lines in are shown in blue.

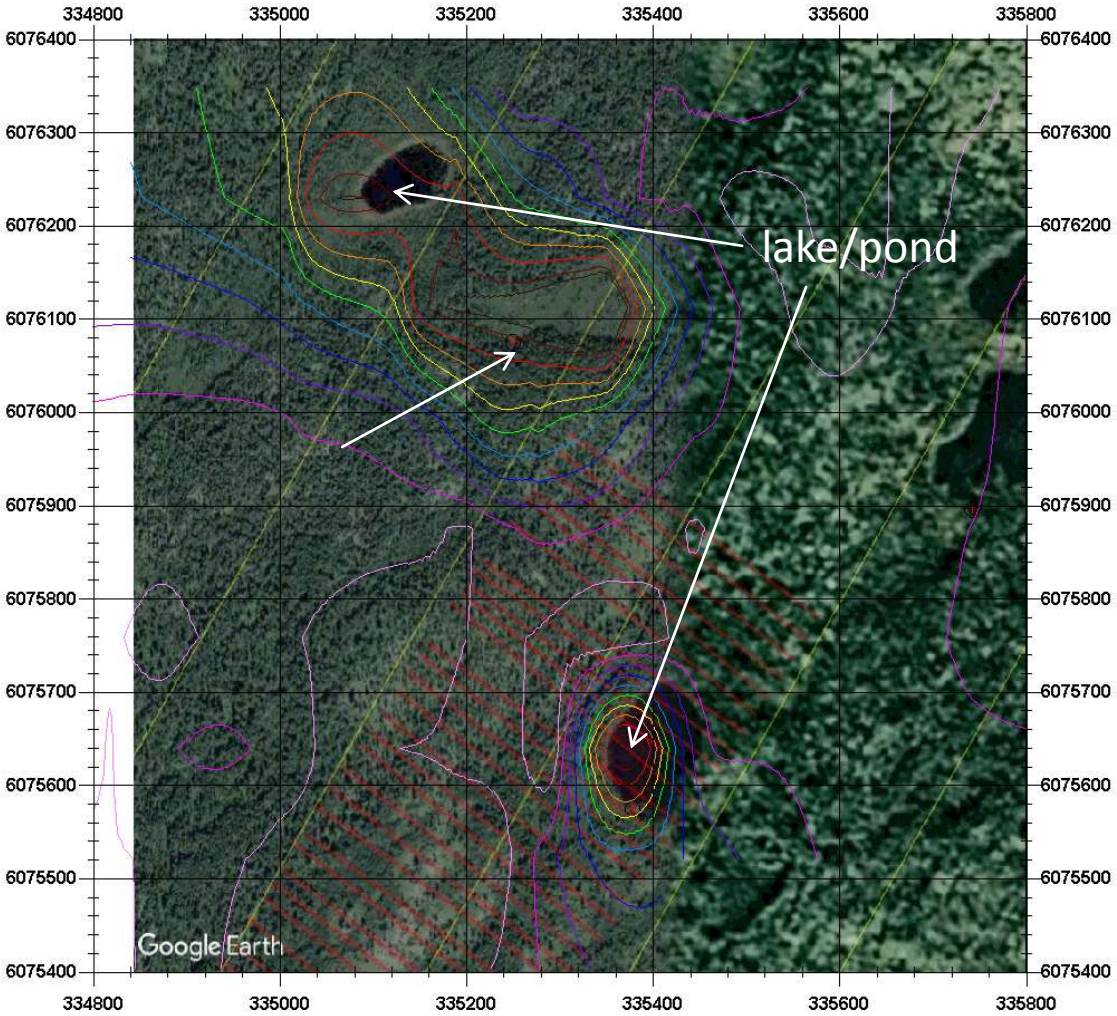

Figure 44 – Ground features as illuminated by the early time VTEM

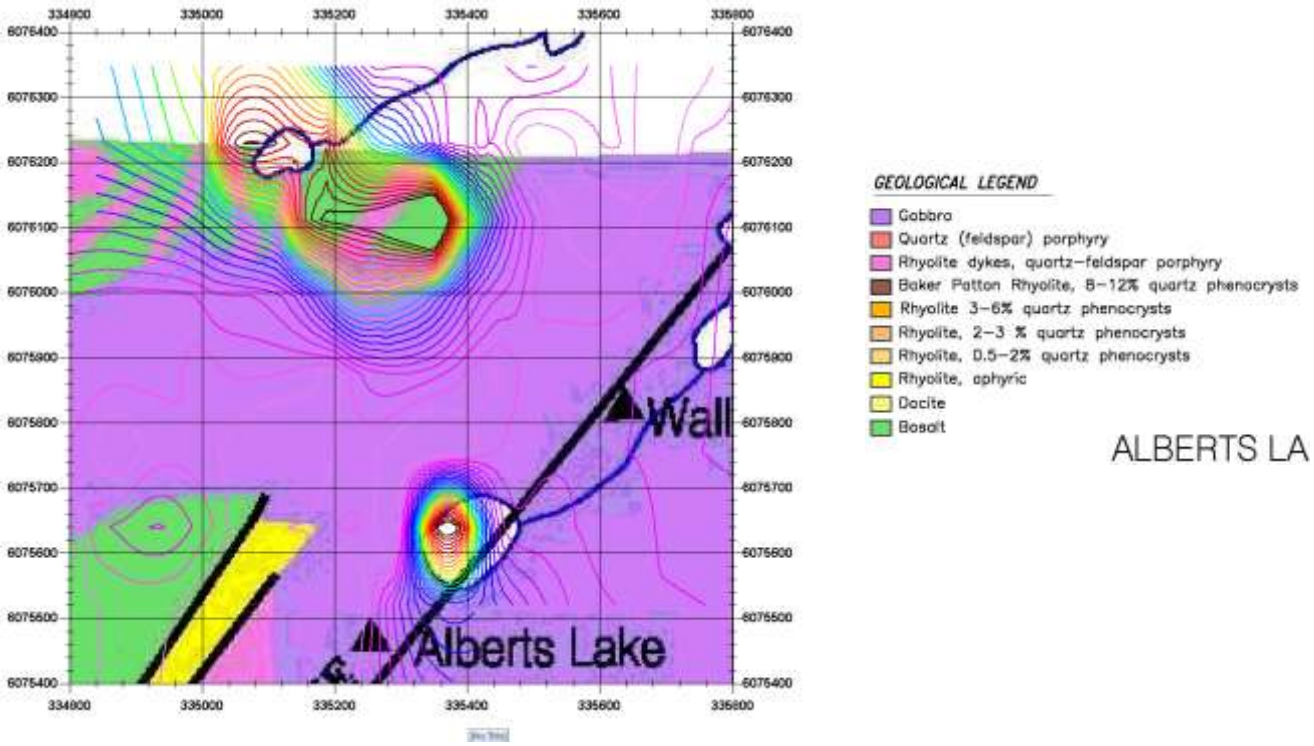

Figure 45 – VTEM Ch5 vs Geology

Here the same early channel (CH5) but with a VLF grid underlay (Fig 45 and Fig 45). These early decays are typical of conductive cover or lake sediments.

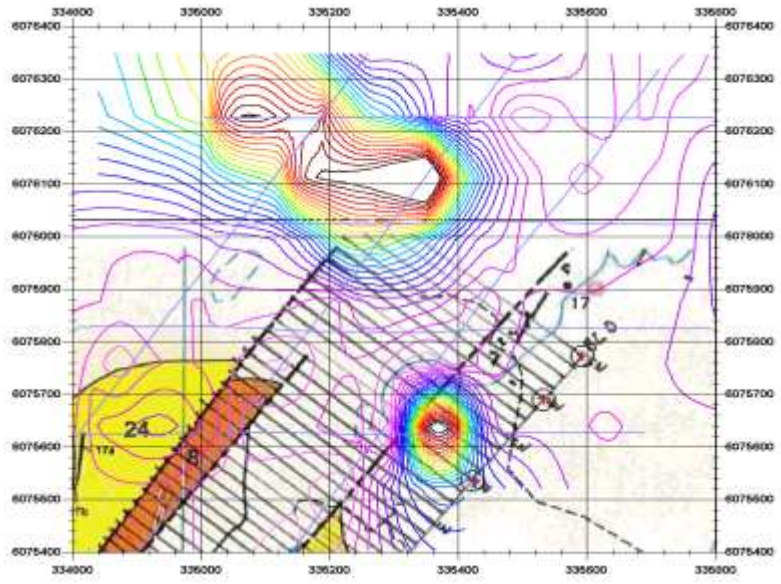

Figure 46– VTEM Ch5 with VLF grid and geology underlain

However, as the time becomes later in the VTEM data, the anomaly feature changes extending EW and southward. Geotech indentified 4 conductors in the area. These conductors are picks along individual profiles and are generated based up the decay rate of the data. As most data beyond Ch5 is noise, the difficulty in such picks is not to pick everything that is not decay. The 4 picks were given the same name "Z4" indicating possibly that the processor viewed them as the same conductor. Our analyses indicates the almost certainty that these 4 picks are simply clipping the edges of this target.

In Figure 47, we show Ch 16 (0.8msec) which is a late early time response. The 4 green dots indicate the center locations of the Geotech Z4 picks. Figure 48 displays a quite late time response at Ch24 indicating a quite slow decay and the possibility of an extension deeper into the VLF grid following the high in the surface magnetics.

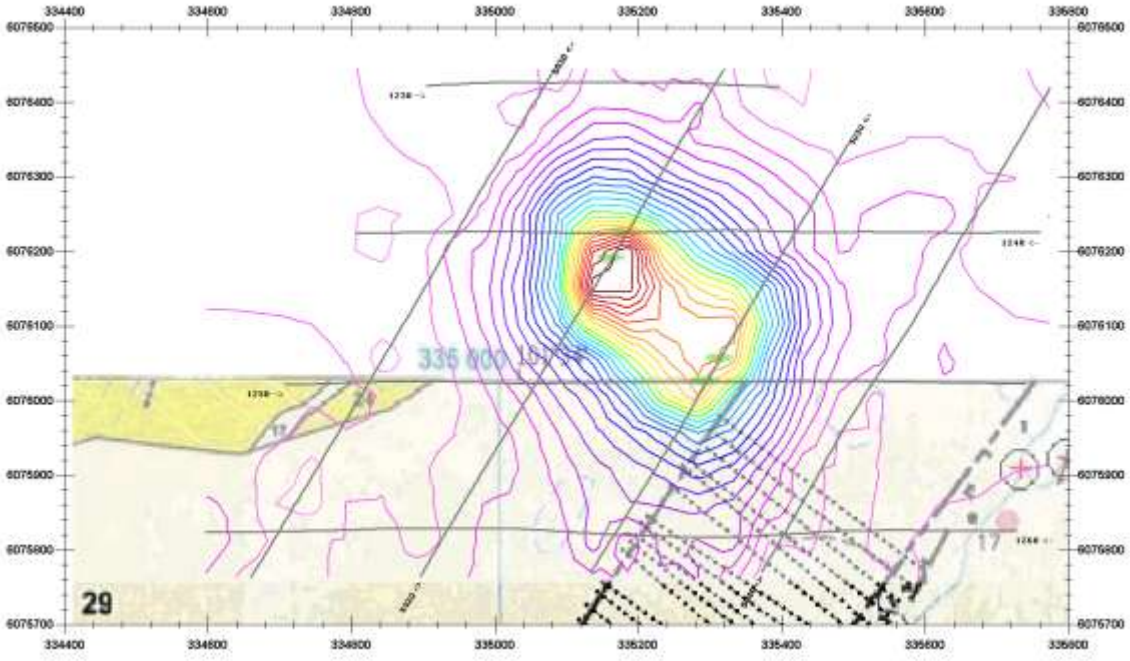

Figure 47– VTEM Ch16

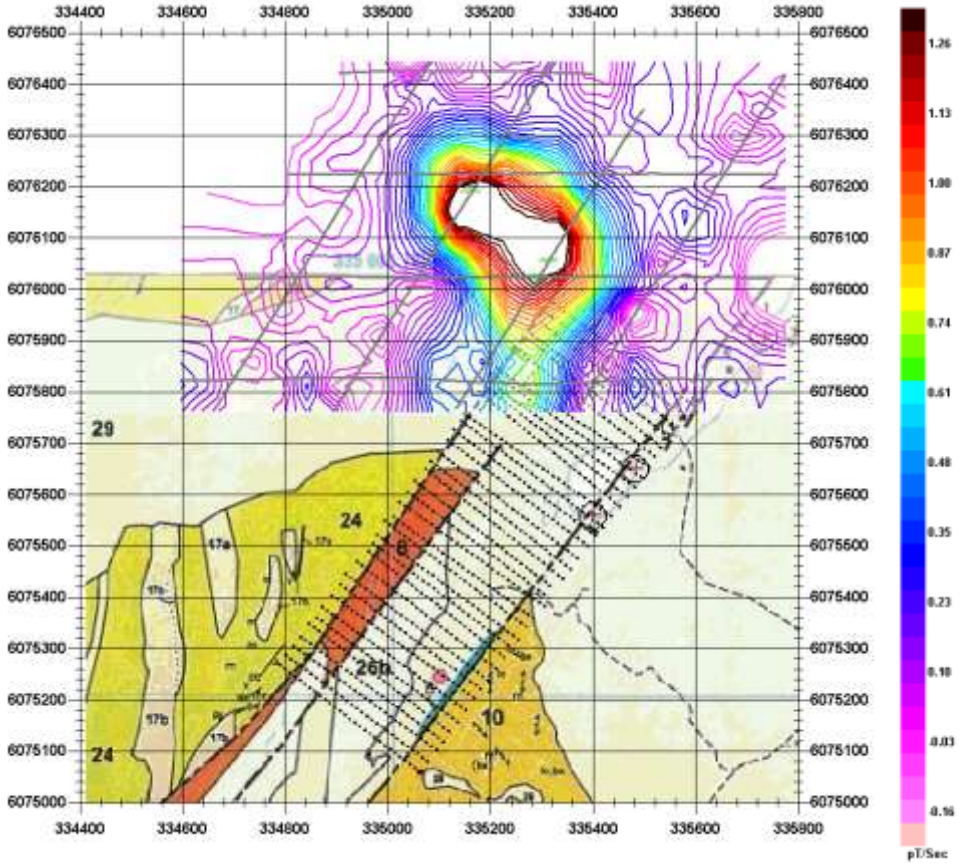

Figure 48 – VTEM Ch24 (2.3msec)

To emphasize that the contour display is not just an artifact of gridding and contouring, we show the figure below (Fig 49). In this figure, we contour Ch18 but also display the actual data is the same colour range at the positions of the data as provided by Geotech. For this channel, the data is well above noise levels.

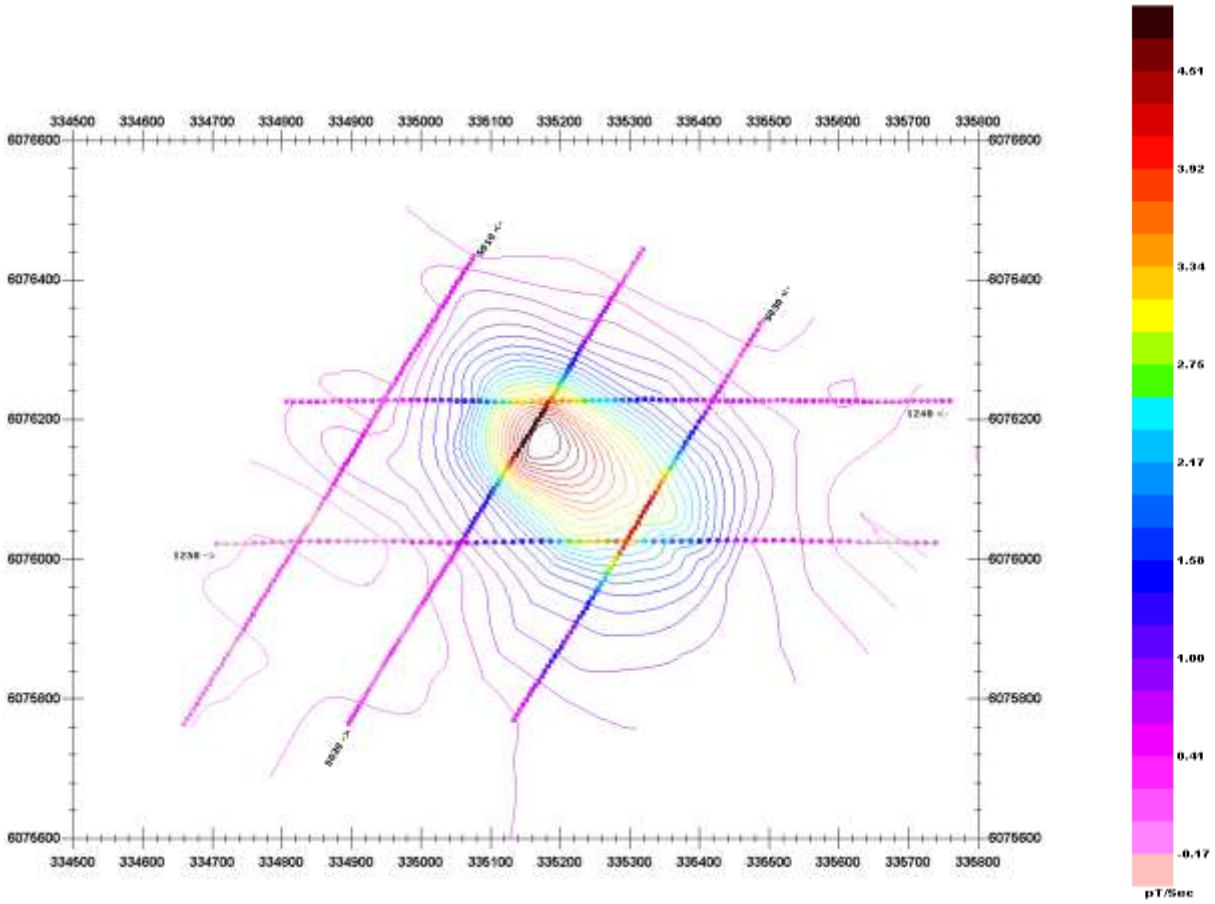

Figure 49 – VTEM Ch18 contours and actual point data

Z4 VTEM Feature

To understand the nature of the response along these sections of the 4 survey lines (5020, 5030, 1250 and 1240), we will look at a data at a selection of data points along 5030. As we proceed south in the plot along L5030, we are moving approximately 50m south or about 70m SW along the survey line. At the north end, the signal is strong but by the southern end, we reduce to the typical response away from any conductors which is essentially noise (Fig50).

At the northern end (red), there is a very quick early decay as is observed over a lot of the surficial conductors. But, we can see along this station (6076125), that the decay slows down around Ch6 and stay quite constant until it becomes noisy. Stations close to this station show less of the surficial response (blue, green) but the same mid- to late-time slower decay. The mid-time decay rate is common to all stations along the edges of this feature. The fact that the

mid to late time decay rate is observable in the data at about an altitude of 40m would indicate that the structure is about the size of the contoured anomaly. Some modeling has been done. The modeling indicates a structure at about 200m depth with an average conductance of approximately 15 Siemens.

Our recommendations are to carry out additional modeling in order to determine the depth and conductance of the anomaly as well as its relationship to the surrounding magnetic high.

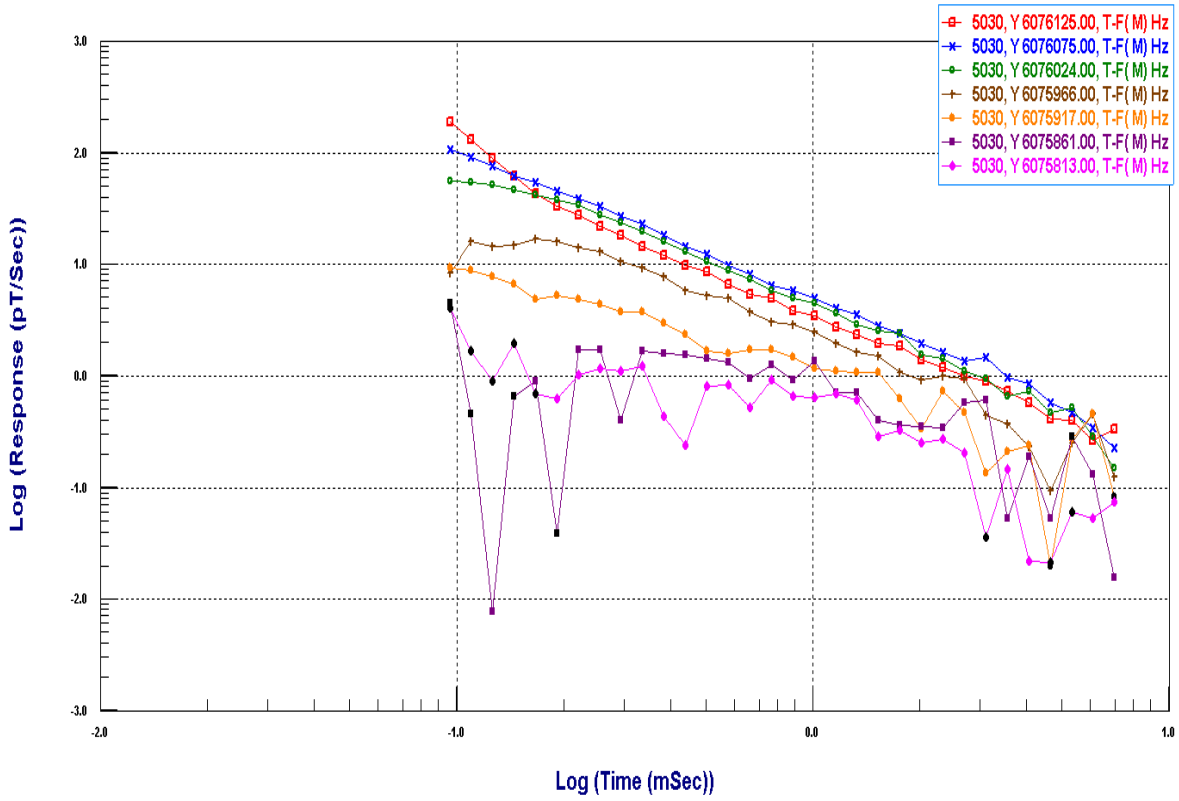

Figure 50 – VTEM decays along L5030.

NW Anomaly (Z4) Model and Suggestions for further Work

With this limited sampling of the response of this anomaly via the airborne data, we have assumed a contiguous body of which the Geotech picks only clips the response. However, the decays along the 4 lines which show a response agree with the model characteristics. Model simulation was done with FSEikPlate, a very accurate plate modeling program.

NW Anomaly:

Strike: 125m at 44 deg NE

Dip Extent: 450m at 1 deg SE

Depth to Top: 200m

Conductance: 50 Siemens

The structural size and conductance is a reasonable VMS target.

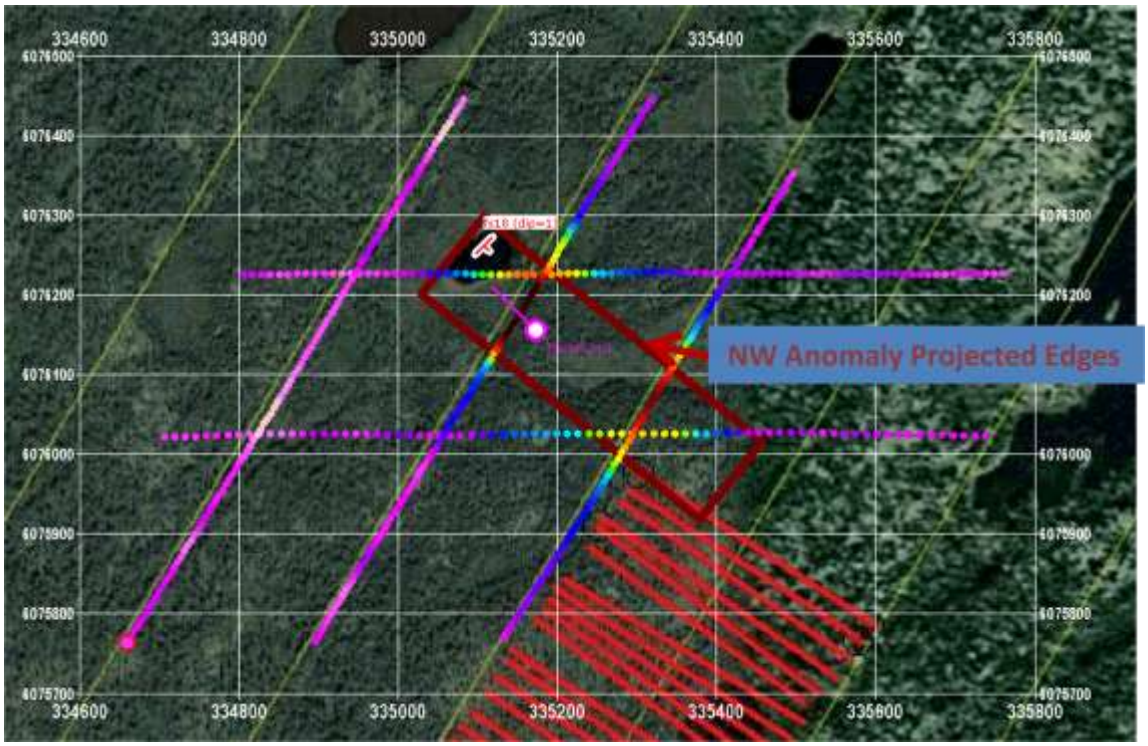

Figure 51 – NW Anomaly outline and suggested borehole

Figure 51 shows the VTEM survey lines with response at channel 20 with the outline of the best fitting model in reddish brown. The suggested borehole is given in pink. Figure 52 shows the model (red) in 3D, with the borehole and the VTEM data lines over the target.

As mentioned, the data sampling of the anomaly is only limited. A ground TEM survey would be recommended. But, we have suggested a probing borehole for the target

Borehole
Collar: 335173E, 6076156N
Dip: 75 degrees
Azimuth: 45 degrees NW
Depth: 300m

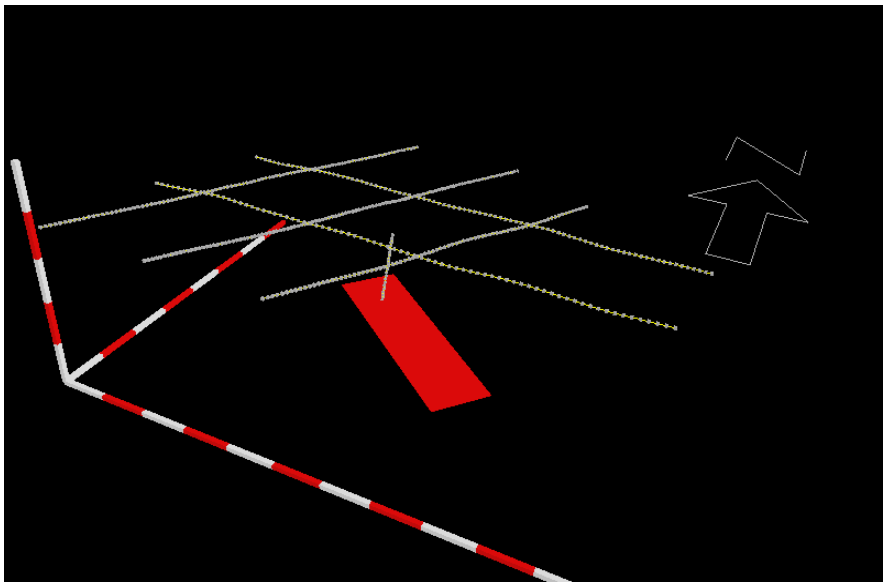

Figure 52 – NW Anomaly 3D view with VTEM lines and borehole

Suggestions for Grid Extension

The ground grid extension is to the north of the previous grid. The line azimuth is as in the previous survey at 35 degrees west of north. The first 3 lines to the south (L450,L475,L500) repeat the previous survey but the profiles extend NE to a length of 750m. In total there are 15 lines (L450 to L800) each of 750m length. Station spacing remains at 12.5m and the line spacing remains at 25m. The grid is 350m in the NE direction and is a total of 11.25 line kilometres. Figure 53, shows the new lines coloured by station with the previous grid in red and a satellite image underneath.

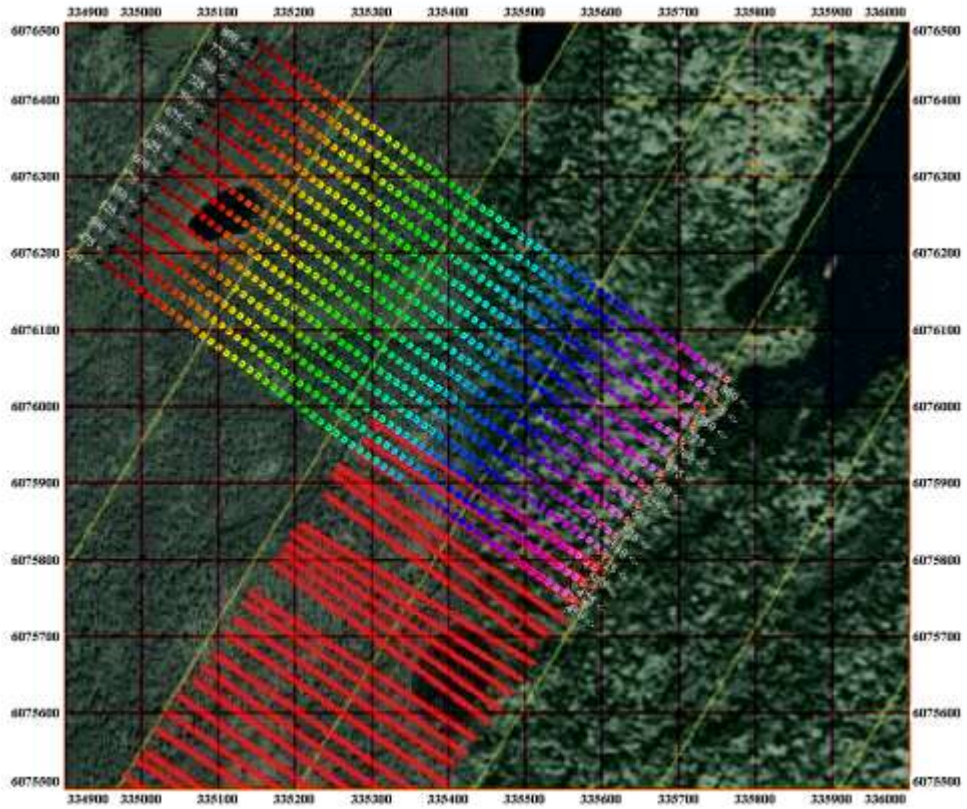

Figure 53 – Grid Extension with 2018 grid in red

Figure 54 is a map of the grid extension with the VTEM aeromagnetic TMI shown underneath to show the relation of the new grid to the strong magnetic feature shown in the aeromagnetics.

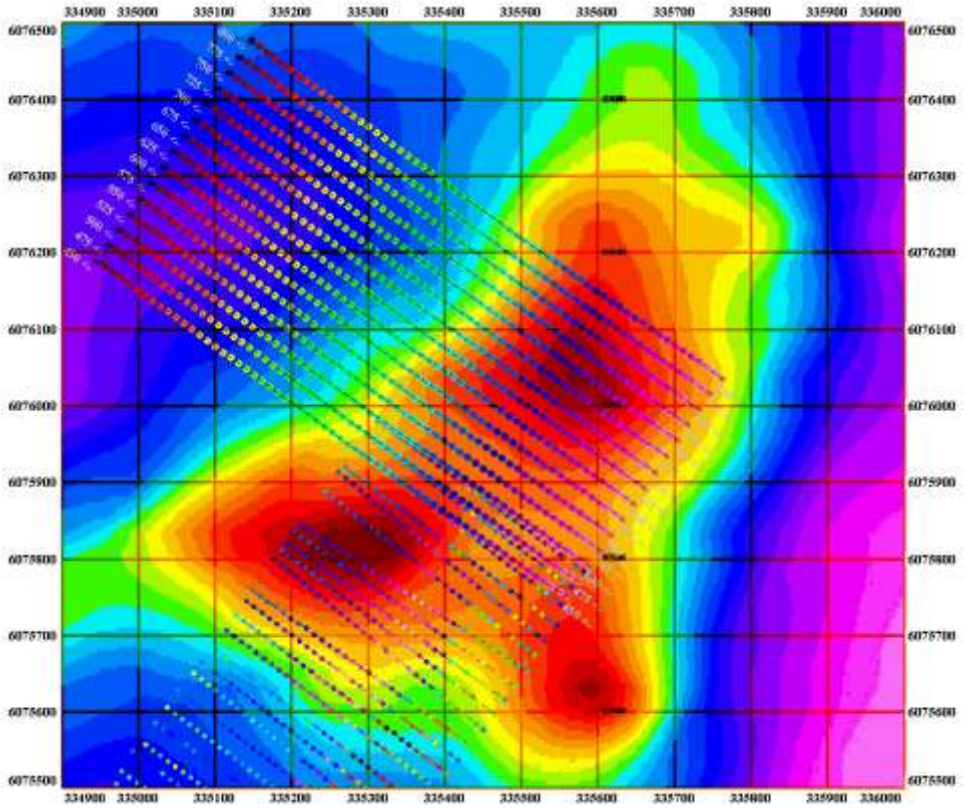

Figure 54 – Grid Extension with aeromagnetic total field underlain

GRID EXTENSION
grid angle – 35 degrees west of north
15 lines – 750m long
12.5m station spacing
25m line spacing
750m by 350m
11.25 line kms total

Figure 55 is a map of the grid extension with the surface projection of the modeled NW Anomaly shown below in blue. The location of the VTEM data used for the model is also displayed. Figure 56 is the grid extension with the geology underlain.

Figure 55 – Grid Extension with NW anomaly underlain

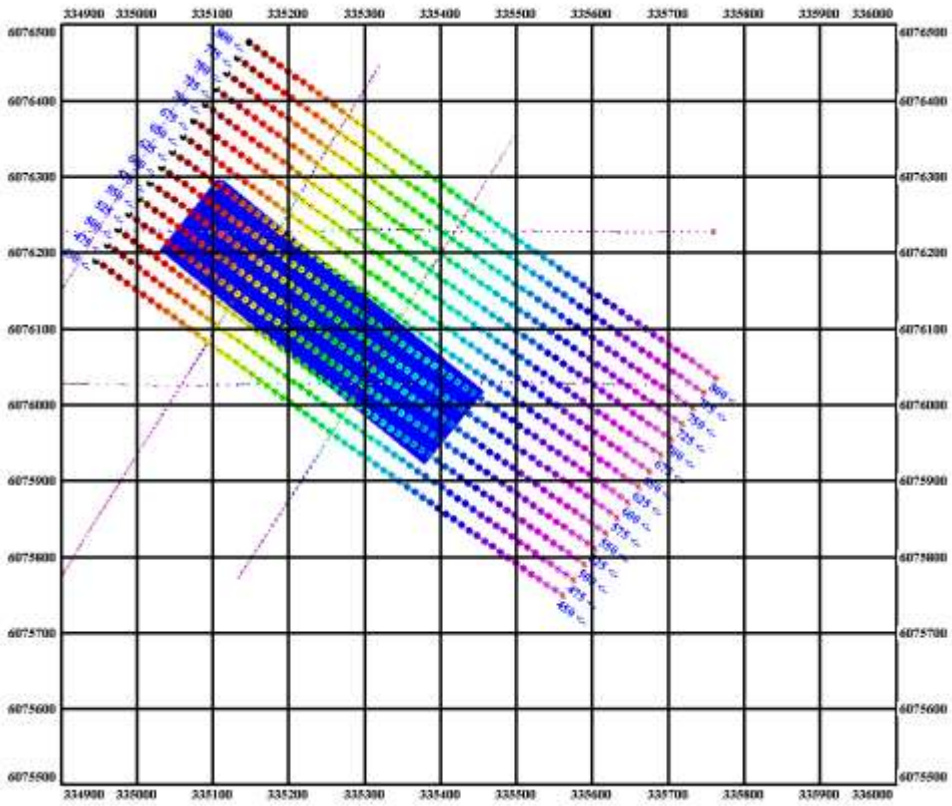

Figure 56 – Grid Extension with geology underlay